Mr

by Shubham Jha

Submission date: 10-Dec-2025 03:14PM (UTC+0530)
Submission ID: 2842210802
File name: 1765301335336_Shubham_Kumar_Thesis.pdf (4.09M)
Word count: 24026
Character count: 134314

MAJOR PROJECT REPORT

ON

EXPERIMENTAL STUDY OF TRIBOLOGICAL PERFORMANCE OF LASER TREATED STEEL SURFACE WITH SMART COATING UNDER THE VIBRATIONAL LOADING

SUBMITTED IN PARTIAL FULFILLMENT OF THE REQUIREMENTS

FOR THE AWARD OF THE DEGREE

OF

MASTER OF TECHNOLOGY

IN

COMPUTER AIDED ANALYSIS AND DESIGN

SUBMITTED BY

SHUBHAM KUMAR JHA

(2K23/CAD/10)

UNDER THE SUPERVISION OF

Prof. R.C. SINGH & Dr. Krovvidi Srinivas

DEPARTMENT OF MECHANICAL ENGINEERING

DELHI TECHNOLOGICAL UNIVERSITY

(Formerly Delhi College of Engineering) Bawana Road, Delhi 110042

JUNE,2025

DEPARTMENT OF MECHANICAL ENGINEERING
DELHI TECHNOLOGICAL UNIVERSITY
(Formerly Delhi College of Engineering)
Bawana Road, Delhi-110042

CANDIDATE'S DECLARATION

I, SHUBHAM KUMAR JHA, Roll No. – 23/CAD/10 student of MTech – Computer Aided Analysis and Design (Department of Mechanical Engineering), hereby declare that the project Dissertation titled "EXPERIMENTAL STUDY OF TRIBOLOGICAL PERFORMANCE OF LASER TREATED STEEL SURFACE WITH SMART COATING UNDER THE VIBRATIONAL LOADING" which is submitted by us to the Department of Mechanical Engineering, Delhi Technological University, Delhi in partial fulfilment of the requirement for the award of degree of Bachelor of Technology, is original and not copied from any source without proper citation. This work has not previously formed the basis for the award of any Degree, Diploma Associateship, Fellowship or other similar title or recognition.

Place: Delhi
Date: 30/05/2025

SHUBHAM KUMAR JHA
(2K23/CAD/10)

DEPARTMENT OF MECHANICAL ENGINEERING
DELHI TECHNOLOGICAL UNIVERSITY
(Formerly Delhi College of Engineering)
Bawana Road, Delhi-110042

CERTIFICATE

I hereby certify that the Project Dissertation titled " EXPERIMENTAL STUDY OF TRIBOLOGICAL PERFORMANCE OF LASER TREATED STEEL SURFACE WITH SMART COATING UNDER THE VIBRATIONAL LOADING " which is submitted by Shubham Kumar Jha, Roll No. –23/CAD/10 here, Department of Mechanical Engineering, Delhi Technological University, Delhi in partial fulfilment of the requirement for the award of the degree of Master of Technology, is a record of the project work carried out by the student under the Prof. R.C. Singh & Dr. Krovvidi Srinivas supervision. To the best of my knowledge and belief this work has not been submitted in part or full for any Degree or Diploma to this University or elsewhere.

Place: Delhi
Date: 30/05/2025

Prof. R.C. Singh
SUPERVISOR

Dr. Krovvidi Srinivas
Co- Supervisor

DEPARTMENT OF MECHANICALENGINEERING
DELHI TECHNOLOGICAL UNIVERSITY
(Formerly Delhi College of Engineering)
Bawana Road, Delhi-110042

ACKNOWLEDGEMENTS

I wish to express our sincerest gratitude to Prof.R C Singh for his continuous guidance and mentorship that he provided us during the project. He showed us the path to achieve our targets by explaining all the tasks to be done and explained to us the importance of this project as well as its industrial relevance. He was always ready to help us and clear our doubts regarding any hurdles in this project. Without his constant support and motivation, this project would not have been successful.

I would also like to extend my heartfelt appreciation to Dr. Krovvidi Srinivas & Prof. B.B. ARORA, Head of the Department of Mechanical Engineering, for his support and encouragement. His vision and leadership have provided a conducive environment for academic and research pursuits. I am grateful for his valuable insights and guidance that have contributed to the overall success of this project.

Lastly, I would like to acknowledge my family & friend for unwavering support, encouragement and understanding throughout this research endeavour. Their love, belief in my abilities, and motivation have been the driving force behind my perseverance and determination.

Place: Delhi
Date: 30/05/2025

Shubham Kumar Jha
2k23/CAD/10

Abstract

High-performance materials such as stainless steels and nickel based super alloys are widely used in demanding applications where high mechanical and thermal properties are required. The applications of super alloys are mainly found in jet engines, power plants and gas turbines demanding high fatigue strength, corrosion and oxidation resistance as well as wear resistant properties. In order to use them, they go through various machining processes such as milling, turning, cutting, polishing etc. until the final product is achieved. Modern manufacturing industries employs various machining tools and technologies to improve the machining process of heat resistant super alloys. However, there are still challenges which needs to be addressed. Among them, adhesive wear of the machining tools is one of the main wear mechanism during the tribological interaction of tool and workpiece, preventing them to achieve the desired quality and surface finish of the end product. Moreover, it damages the tool reducing its lifecycle and in return, increasing the production cost. Among the cutting tools tungsten carbide (WC/Co) tools coated with TiAlN coating due to their good high temperature performance are extensively used. Nonetheless, these coatings still face issue like adhesive wear, abrasion, oxidation at higher temperature damaging the tools and subsequent machining. Therefore, it is imperative to understand the initiation mechanism of adhesive wear during the tribological interaction of super alloys and coated cutting tool material.

In this research work, the tribological response of two coatings deposited by physical vapour deposition (PVD), having the composition $Ti_{60}Al_{40}N$ and $Ti_{40}Al_{60}N$ have been studied against two super alloys material, i.e. Inconel 718 and stainless steel 316L. A high temperature SRV (Schwingung (Oscillating), Reibung (Friction), Verschleiß (Wear)) reciprocation friction and wear test set up was employed to investigate the friction behaviour, wear rate and dominant wear mechanisms.

For $Ti_{60}Al_{40}N$ coating, the experimental results revealed that generally, friction increases in case of sliding against Inconel 718 up to 400 °C and drops at 760 °C. A high wear volume at room temperature and a decrease to a minimum at 760 °C has been observed for Inconel 718. On the other side, Stainless steel 316L (SS 316L) faces a continuous rise in friction coefficient with highest value at 760 °C during sliding against $Ti_{60}Al_{40}N$ coating. Wear is highest at 400 °C for SS 316L pin. The worn surfaces shows that both workpiece materials experience increase in material transfer due to adhesive wear with rise in temperature. At 400 °C, adhesion is the primary wear mechanism for both workpiece materials. A further rise in temperature to 760 °C promotes the adhesive wear through oxides formation on both material surfaces.

Similarly, $Ti_{40}Al_{60}N$ coating shows the same friction behaviour with change in average steady state friction values for both material of Inconel 718 and SS 316L. Both workpiece materials responds in a similar way to wear volume loss, i.e. lowest at room temperature and highest at 760 °C. For Inconel 718, transfer of coating constituents on to the Inconel 718 pin surface was detected and associated with coating rupture and peeling, exacerbating with rise in temperature. Adhesion, abrasion, and oxidation are primary wear mechanisms at 400 °C and 760 °C. For SS 316L, coating

transfer only happen at 400 °C. No damage of coating at 40 °C, a complete damage at 400 °C, and formation of dense porous oxides layers at 760 °C have been noticed. At 400 °C, adhesion, abrasion, and chipping while at 760 °C, adhesion, three body abrasion, ploughing and oxidation are the main wear mechanisms.

Additive manufacturing has revolutionized component fabrication by enabling the production of complex geometries and tailored surface textures unachievable by traditional methods. However, AM surfaces often exhibit intrinsic roughness, porosity, and microstructural heterogeneity, which can detrimentally affect frictional characteristics and accelerate wear under operational stresses. To mitigate these drawbacks, laser surface treatment is employed as an effective post-processing technique to modify surface hardness, induce compressive residual stresses, and homogenize surface microstructure, thereby improving wear resistance and mechanical integrity. The incorporation of advanced smart coatings—such as magnetorheological fluids and shape-memory polymers—further enhances the tribological system by providing adaptive vibration damping and frictional modulation capabilities, which are particularly advantageous in high-frequency vibrational environments.

The research methodology involves detailed finite element analysis (FEA) using ANSYS Workbench, simulating a representative pin-on-disk tribological configuration under dry sliding conditions coupled with various vibrational load profiles. Comparative simulations across three primary surface conditions—untreated AM, laser-treated, and smart-coated laser-treated surfaces—are conducted to quantify and analyze key tribological metrics including coefficientof friction, wear depth, contact pressure distribution, and vibrational response characteristics. The simulation results reveal a marked improvement in tribological performance for laser-treated and smart-coated surfaces, exhibiting reduced frictional forces, diminished wear rates, and superior vibration attenuation compared to conventional AM surfaces. These findings elucidate the synergistic effects of combining advanced manufacturing, surface engineering, and smart material technologies to realize robust, adaptive, and long-lasting tribological systems.

Table of Contents

Table of Figures

List of Tables

Chapter 1

1. Introduction

From the beginning of the history and initial days of the human evolution, materials have been of crucial importance for making development in our society. The slow and gradual improvement has not only carved society as we know it today, but also made us pave the way towards various technological advancements in different scientific domains such as space technology, energy, transportation, medicine, and communication.

Arguably, steel has been deemed as the most central material in the expansion and development of humanity. This versatile and multi-functional material has not only played a pivotal role in our civilization and economic growth but also prompted the industrial revolution since the first inexpensive method of mass production of steel was revealed in 1855 by Henry Bessemer [1].

Now a days, most of the materials used in the manufacturing industry comprises of steel. In manufacturing industry, the ability to change the shape of steel according to requirements is one of the key aspects of its widespread utilization. For example, steel usage in construction industry, heavy machinery, bridge construction against heavy floods, power plants and automotive sector makes it one of the most promising and reliable material being justified with its longer life and durability. Therefore, steel due to its robust strength, toughness and stiffness is not only the backbone of various technological advances that has been witnessed in today's era but also have played vast role in rising up our living standards [2, 3].

Over time, it has been realized by engineers that addition of different elements to the composition of metals for producing alloys can change its properties significantly. Traditional metal alloys such as steel or aluminium when used in different areas such as automotive, heat treating, nuclear power generation, gas turbines, and jet engines makes them prone to failure at very high temperatures. Therefore, high temperature capability alloys which are resistant to failure at very high temperature with very good corrosion and creep resistan as well as significant fatigue strength are required. The super alloys can mainly be categorized into three classes; nickel based, cobalt based, and iron based super alloys are prominent for applications at severe conditions. However, each category has different subsections depending on the composition of the added elements as well as the specific requirement for application [4, 5].

Until the end of the 3rd decade of the 20th century, engineers and designers realized that stainless steel utilization is limited by the high temperature requirement a they need to come up with another solution for high temperature applications from where the nickel based super alloys usage originated. Nickel based super alloys are extensively used for harsh operating conditions, e.g. in jet engines as depicted in Figure 1, where high stability against acid attack, oxidation, corrosion, fatigue, and creep is required [6]. The ability to withstand high temperature in nickel based super alloys comes from the precipitation of high-volume fraction of nitrogen triiodide (Ni_3) [7].

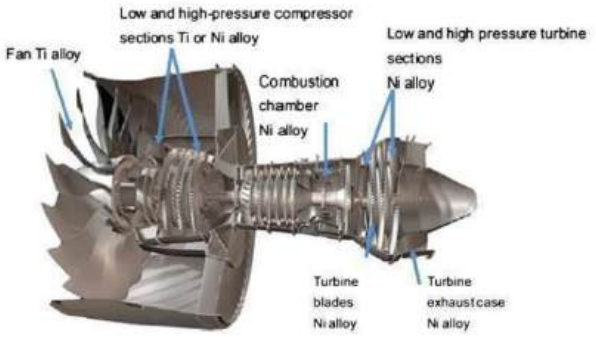

Figure 1: Use of the nickel alloys in jet engine is around 45-50% of its total weight [8]

Among the super alloys, as each group has variation in chemical and mechanical properties controlled by varying the alloying element and heat treatment process. Stainless steel and Inconel are the famous ones holding the mark for standing robust at high temperature application by retaining excellent mechanical properti[63] It is important to mention here that sometimes Inconel is employed in place of stainless steel due to its high resistance to creep and corrosion and acid attack at very high temperatures [9]. The classification of super alloys has been shown in Table 1.

Table 1: Super alloys classification [10]

SUPER ALLOYS		
NICKEL BASE	**IRON BASE**	**COBALT BASE**
Inconel (587, 597, 600, 601, 617, 625, 706, 718, X750)	Incoloy (800,801, 802,807, 825,903,907, 909)	Haynes 188
Nimonic (75, 80A, 90, 105, 115, 263, 942, PE.11, PE.16, PK. 33)	A-286	L-605
Rene (41, 95)	Alloy 901	MAR-M918
Udimet (400, 500,520, 630, 700, 710, 720)	Discaloy	MP35N
Pyromet 860	Haynes 556	MP159
Astroloy	H-155	Stellite 6B
M-252	V-57	Elgiloy
Hastelloy (C-22, G-30, S, X)		
Waspaloy		
Unitemp AF2-IDA6		
Cabot 214		
Haynes 230		

The evolving world and developing societal requirements have completely shaped the manufacturing industry. Multiple driving forces are considered behind this change including environmental change, access of technology, globalization, customer requirements, and enhancement of knowledge. The manufacturing of quality products to achieve sustainability and less pollution due to environmental concerns has increased the machinability of materials. In these engineering materials, machining of super alloys causes inordinate generation of heat, compromised surface features, wear in sufficient amount, and also residual stresses specifically corresponds to materials which are not easy to machine [11].

1.1. Machining of Super alloys

Machining of materials is usually dictated by the chemical and mechanical properties governing the difficulty level of machining process. Researchers have classified the engineering materials into small category-based nature of machining process, i.e. (i) easy machining materials, (ii) machining of the ordinary iron and wrought steel, and (iii) materials which are difficult to machine. With the growing demand of customer satisfaction, challenges are often encountered in order to ameliorate machining efficiency without compromising the final product quality and reducing the cost [12].

The competitive market of today's industry considers machining of materials as one of the key manufacturing processes. This leads to the development of the state-of-the-art standards for machining processes. As the innovation is taking place with fast pace with new methods entering into the market, different techniques, for example, high speed machining, micro machining, and ultra-precision machining offer wide varieties in the machining processes. In the current industrial market, the machining process not only aims for efficiency and high production rate but also improved suitability, reliability, and economy [5, 9].

1.2. Challenges in Machining of Super alloys

In the machining of materials, super alloys are considered to be the most difficult to machine. Nickel and iron based super alloys have high resistance to corrosion and oxidation, and are used in high temperature applications in various industrial sectors. Besides the super alloys, stainless steel 316L is a difficult to machine material as it poses various challenges during its machining. The work hardening characteristics combined with low thermal conductivity as shown in Figure 2 and high ductility renders stainless steel 316L to wear out the tool by chipping out the material from cutting tool. As a result, the tool life reduces and quality of the product gets compromised leading to increased cost of machining process [14]. Many researchers like Ranganathan et al. [15] has made efforts to investigate low cost methods for machining of the materials e.g. duplex stainless steel and AISI 316L. Researchers such as Nomani et al. [16] have found out and reported that low thermal conductivity is the main reason behind the poor machinability of stainless steel. Similarly, different machining techniques and methods were used to improve the machinability of stainless steel involving cryogenic treatment for increasing the tool life. For example, Gill et al. [17] used the cryogenic treatment method for the uncoated WC-Co tool at two different temperatures i.e. shallow treatment at -110 °C and deep treatment at -190 °C, and has observed

increased cutting tool life and machining performance as compared to the untreated tool WC-Co cutting tool. Laizhu Jiang et al. [18] investigated the machining of the stainless steel and duplex steel and found that serration of the chips leading to the vibration of the cutting forces enables attrition wear on the cemented carbide cutting tools. Little work has also been reported that the excessive heat generation causes the strong bonding between the workpiece and the tool material causing the adhesive wear.

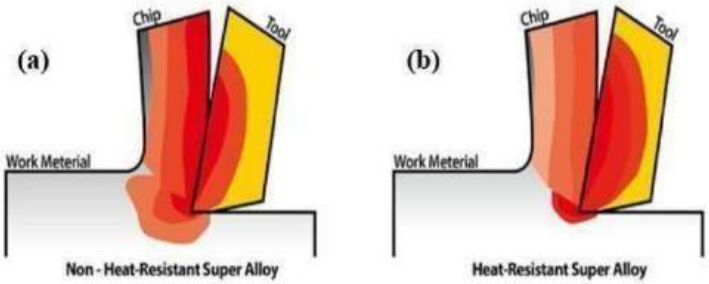

Figure 2: Machining of super alloys (a) transfer of heat to work material leading to less heat accumulation at the contact point (b) back transfer of heat to the tool surface resulting in rise of tool temperature enabling wear [19]

Adding more to it, some scientific studies conducted by researchers have reported different challenges during their experimental study which they believed could be the plausible reason for the poor machinability of the austenitic stainless steel. Enomo et al. [20] mentioned in his findings that the poor machinability of austenitic stainless steel can be attributed to the presence of the macro particles on the surface of the AlTiN, AlCrN PVD coated tool. The non-homogeneous formation of the chip during the machining of the AISI 304 austenitic stainless steel has been found to be the leading cause of its poor surface finish as being reported by Korkut et al. [21]. Also, the work by Akasawa et al. [22] on machining of austenitic stainless steel accounts for achieving a high surface roughness when re-sulfurized steel is used and this generate further built-up edge (BUE). Lin [23] looked at the machining of austenite stainless steel from the perspective of grain size and found out that increase in grain size results in poor machinability. He also studied the machining of quenched austenite stainless steel bar and reported that increase in temperature for quenching reduces the quality of machining along with the tool life. Rodriguez et al. [24] analyzed the effect of coated and uncoated tool on machining quality of stainless steel and came to the conclusion that single coated and uncoated tools suffers early failure enabled by the cutting forces which were pretty high during the machining process. Similarly, some researchers like Khan et al. [25] investigated texturing of the surface of the flank and rake face of the cutting tools which has significantly reduced the friction and cutting forces between the tool and work piece that will eventually prolong the tool life. It is observed that employing the texturing technique can enhance the lubrication between the tool and workpiece and affects the chip adhesion phenomenon. It has also been reported that laser machining used for creating the texture on rake face of carbide tools makes them outperform plain carbide tools during the machining of AISI 316 stainless steel [26].

The resistance against oxidation and creep rupture comes from the addition of aluminium and titanium [8]. With all these strengths and characteristics, there are different problems associated with the machining of nickel based super alloys. Many researchers have looked into the dry machining problems and presented them in the literature. For example, Dudzinski et al. [27] presented in their review that plastic deformation, increase in micro-hardness, residual tensile stresses, and metallurgical changes as well as high surface roughness are the leading causes of the poor machinability of the nickel based super alloys. Similarly, Devillez et al. [28] in his experimental investigation about the dry cutting of Inconel 718 explored that Inconel 718 affinity to weld leading to formation of built-up edge (BUE), its increased shear strength, and chemical affinity are major difficulties during its machining process. Likewise, Arunachalam and Mannan [29] analyzed the machining of nickel based super alloys with respect to the nickel (Ni) content in the material and found interesting results. As demonstrated in Figure 3, the cutting temperature during the machining gets high with the rise in the nickel (Ni) content in the super alloys. They also found that notch wear associated with machining of nickel based super alloys also increases when an increase in material hardness has been observed. The machining conditions should always be determined based on the microstructure and chemical composition of the material which is directly linked with the hardness of the material.

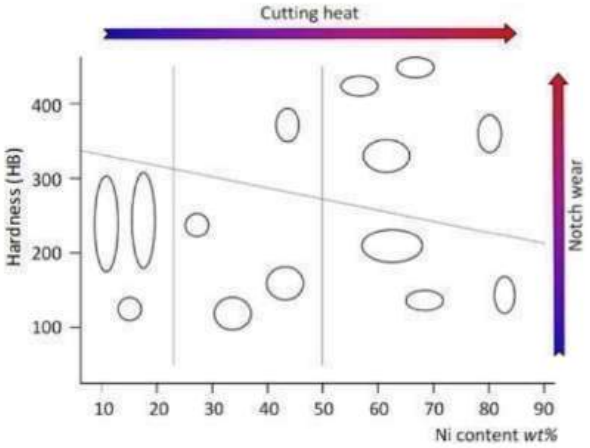

Figure 3: Change in cutting heat and Notch wear with rise in nickel content [29]

Besides the nickel content, it has also been studied by Olovsjö et al. [30] that grain size greatly affects the machining quality of the nickel based super alloys along with the tool wear. They proposed that large grain size in wrought Inconel 718 has almost no effect on the flank wear of the tool, however, it greatly influence the notch wear on the tool and undermines the machining quality and tool life. Hayama et al. [31] focused on the initial tool wear relation with the feed rate and grain size ratio. It was mentioned that if feed rate to grain size ratio is less than 1, flank wear on the tool progresses very fast and relies completely on the mean grain size.

According to Thakur et al. [31], the compression ratio of the chip can also be a good indicator about the machining quality of the Inconel 718. This is due to the fact that it is related to the plastic deformation and the energy consumption during the process of metal cutting. Their studies proposed that for Inconel 718, the plastic deformation was significantly higher which is enabled by work hardening during the turning process. Xavior et al. [32] describes that presence of abrasive carbides in microstructure and along with the very high work hardening characteristic are the leading cause of inconvenience faced during machining of the nickel based super alloys. Some other researchers also demonstrated their finding regarding challenges faced while machining the nickel based super alloys. The performance efficiency of the carbide tools were tested by Noor et al. [33] for machining of nickel based super alloys. Their investigations confirmed the plastic strain and crater wear of the cutting tool edges resulting from the low thermal conductivity, accumulating the generated heat on the tool edge surface, and not transforming it to the workpiece chips. It has also been reported that delamination of the coating occurs with coated tools due to the chemical reaction as well as metal pick-up on the tool surface reducing the life of tool and machining quality. While performing the turning operation of Inconel 718, Ibrahim et al. [34] explained the excessive chipping of the tool along with flank and rake wear due to the brittle nature of the Inconel 718 combined with high speed cutting.

1.3. Tribology

The word tribology is typically not familiar to the common person although it has a very crucial role in our lives. It plays an important part in the behavior of two surfaces in contact when they move relative to each other. Besides the technology-based applications, which are highly dependent on the tribology (i.e. friction, lubrication, and wear), everyday walking also needs proper friction between the ground and the shoe sole to prevent from slipping. Also, the knife blade sharpening is another form of tribology that falls into the category of controlled wear. Similarly, lubrication is also equally important for the proper performance of the working systems, for example, human knee and hip joints.

The scientific definition of tribology is the study of two interacting surfaces that are in relative motion. Tribology entails friction, wear, and lubrication. The origin of the term tribology comes from the Greek word "tribos" meaning "to rub". The word tribology was first mentioned by the Jost report in 1966, which was published by the Education and Science department of United Kingdom. This report highlighted the importance of the tribology and lubrication research in UK's education department with a conclusion that almost 1% of the UK gross product can be saved with decrease in friction as well as wear [35]. Such initiative was also taken by other countries depicting much higher savings resulting from reduction in friction and wear. However, a closer look into history shows that role of tribology and lubrication was also considered even around 2500 B.C during the construction of pyramids and they might have used oil and water mixture as lubricant for reducing the friction.

The modern tribology research is primarily focusing on improved performance and reliability; saving raw materials; energy savings; and cost savings. Figure 4 demonstrates a tribological system from the perspective of different real-life applications. A tribological system mainly consist

of four main components i.e. two interacting surfaces (tribo-element 1 and 2), interfacial material, and surrounding medium. Elements 1 and 2 are basically two surfaces which are close to each other during the actual operating conditions. While the third element is the interfacial medium acting as a lubricant which can be oil, some gas or any layer serving as to reduce friction and wear. The fourth element is the surrounding medium which is usually air entailing humidity as its main impacting factor. Gaseous environments, some fluid or vacuum depending upon the specific requirements and operating conditions of the tribological system can also be the surrounding medium. All the above mentioned four elements serves as the decisive factor concerning the friction and the wear in the tribological system. Therefore, it can be said that friction and wear involved in a tribological system are not its intrinsic material properties but solely depends on the configuration and environment of the tribological system [36].

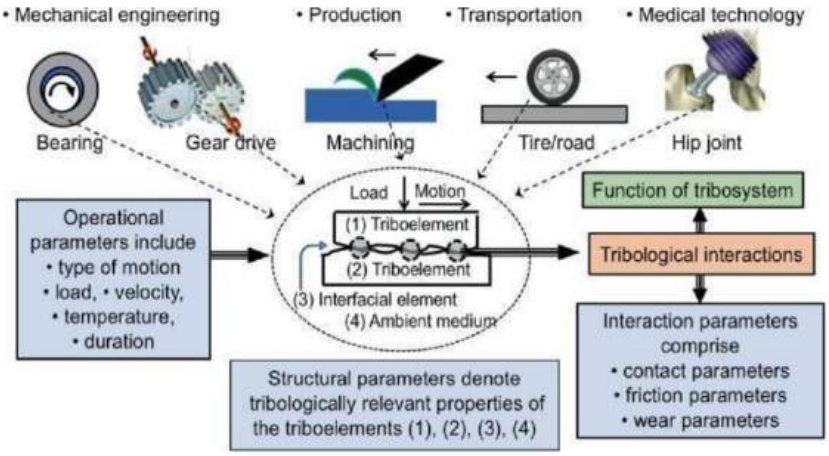

Figure 4: Schematic diagram of a tribological system for various practical configuration [37]

Friction between the two contacting bodies can be attributed to the resistance against the sliding motion. In reality, it is actually the force which tend to oppose or opposes the relative motion between the two mating surfaces. The refore, it can be said that the frictional force is an energy dissipative force. The sliding friction originates from the combined effect of two components of friction i.e. ploughing and adhesion. The ploughing form of friction occurs between two materials of different hardness. In other words, when asperities of the hard surface plough through the soft mating surface. This form of friction can also result from the hard particles entrapped between the two surfaces that are in relative motion. On the other hand, the adhesive form of friction results from the atomic junction formation between the two mating surfaces. The higher chemical affinity of the materials plays significant role to increase this sort of frictional component. For example, two steel surfaces will form atomic bonds during dry sliding contact if there are no oxides layers on the surfaces in contact. It is important to have no oxide layers as oxides reduces the formation of the atomic junctions preventing the adhesive form of friction.

Wear can be described as the loss of material from the surface of the contacting bodies. This does not impart that material should be removed from the tribological system but can transfer from one surface to the other opposite surface. Wear in the tribological system does not favor smooth operation of the system and can result in deterioration of the performance and eventually failure of the system. Therefore, it is always desired to keep the wear as minimum as possible through selection of the appropriate material and lubricants for the required operating conditions. However, wear is not always undesirable as there are manufacturing processes where controllable wear is preferred. Examples of such systems are milling, turning, cutting, and grinding as well as polishing.

There are four main types of the wear as being standardized by the German standards DIN 50320 shown in Figure 5.

— **Adhesive wear:** sometimes also termed as sliding wear. This happens when the formed atomic junctions between the two mating surfaces breaks and the material loss occurs.

— **Surface fatigue wear:** resulting from sub surface cracks formation and fatigue generated from the repeated stress cycles in the tribological system enabling the removal of the material from the contacting surfaces.

— **Corrosive or tribochemical wear:** The consumption of material resulting from chemical reactions on the surface of contacting bodies. In this type of wear, the tribological actions triggers the chemical reaction among the tribological elements of the tribological system.

— **Abrasive wear:** A 2-body abrasive wear occurs when asperities on a hard material surface plough through the surface of a softer material and make scratches on opposite surface. A 3-body abrasive wear is generated by the hard entrapped particles that scratches and plough on one or both of the mating surfaces.

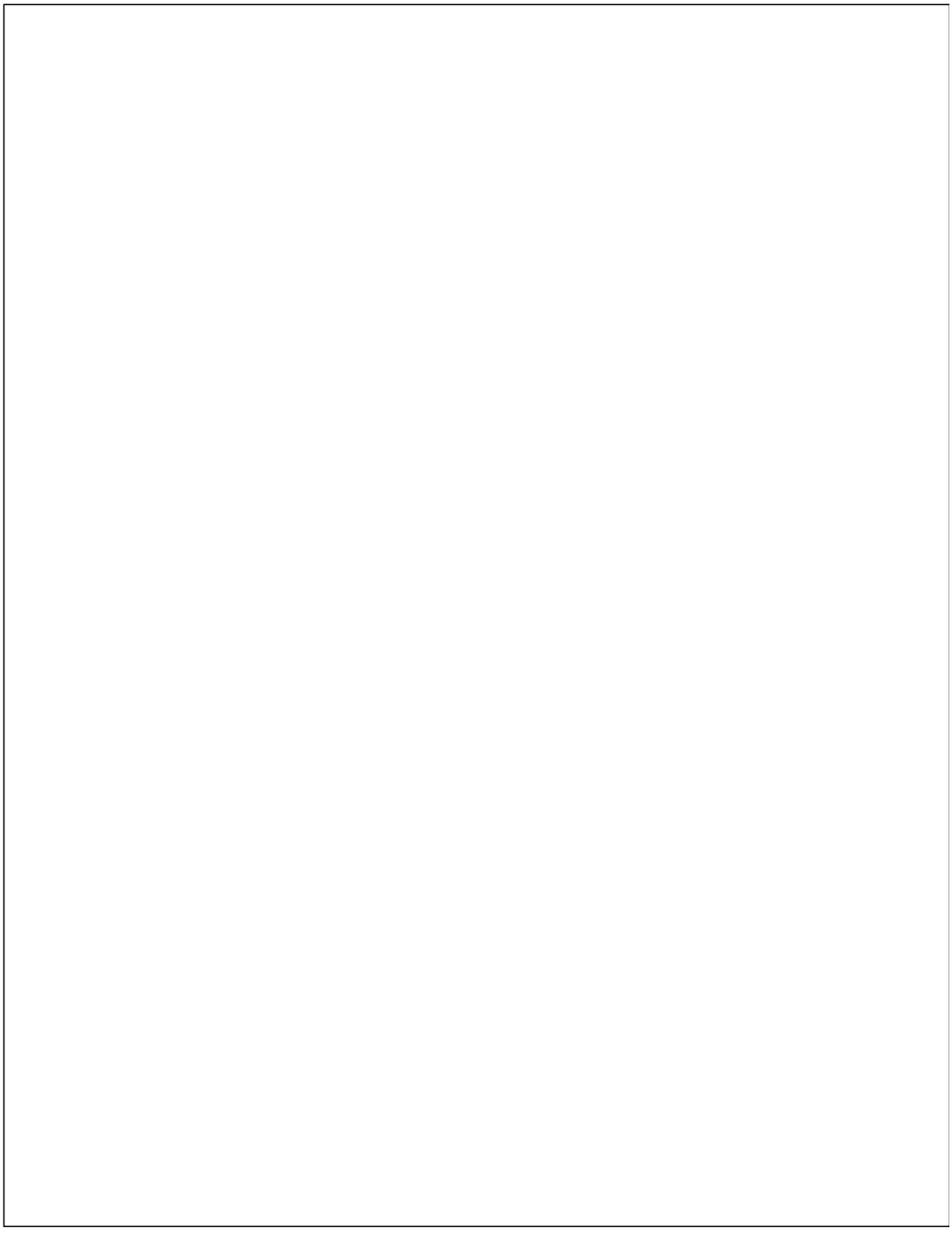

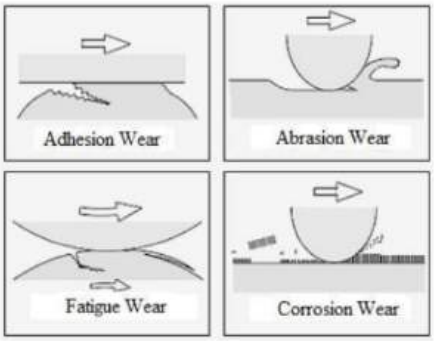

Figure 5: A schematic diagram of four main wear types according to German DIN 50320 Standard [38]

Adding more to it, researchers describe two more wear mechanisms as follows:

— **Erosive wear:** process in which impact of liquid, solid and gases or a combined effect of these removes the material from the surface of the solid material.

— **Fretting wear:** small amplitude oscillatory movement under high loads generates this type of wear between the contacts of two surfaces. The resulting wear particles from the fretting wear don't find any way to get out of the contact region and consequently exacerbate the wear behavior [36].

1.4. Tribology in Machining

The challenges about the machining of the super alloys has previously been discussed in section 1.2. Tribology is also an integral part in the machining process of super alloys e.g. milling, turning, and cutting, as it involves the interaction of the tool and workpiece surfaces when the tool is loaded with high forces during the process of chip formation. The generation of heat at the deformation zones leads to overheating the chip, tool surface, and workpiece. Since all the surfaces are clean and chemically active, therefore complicated physical and chemical processes are linked with cutting process. These processes enable wear of the tool surface which reflects in the form of progressive wear of the particles from the surface of tool. However, defining it in more simple words, tool wear usually comes from the mechanical interaction (thermodynamic wear, in most cases abrasion) and chemical interaction (thermochemical wear, mostly diffusion). The temperature due to excessive heat generation may exceed the limit of the tool and workpiece material resulting in enhanced crater wear, cutting edge chipping or severe damage to the tip of tool [7].

During the machining of the steel and nickel based super alloys, different tool wear mechanisms have been observed such as abrasive wear, adhesive wear, oxidation wear, and diffusion wear.

Among the above mentioned wear mechanisms, adhesive wear is the most frequently occurring one resulting from the combined effect of high temperature and stresses leading to the built-up edge (BUE). The formation of the built-up edge accounts for failure of the tool through attrition phenomenon at medium cutting-speeds. Flaking and chipping as well as plastic deformation are more prominent at higher cutting speed. Figure 6 describes the different wear mechanism along with the wear types.

From literature, it has been observed that adhesion and abrasion are the most frequently occurring tool wear mechanism during the machining of the nickel based super alloys. The leading cause of this are the high cutting forces which enables this mechanism not only at low temperature but also at high temperature as well [39]. A brief yet compact summary of the various wear mechanisms has been described during machining of the super alloys.

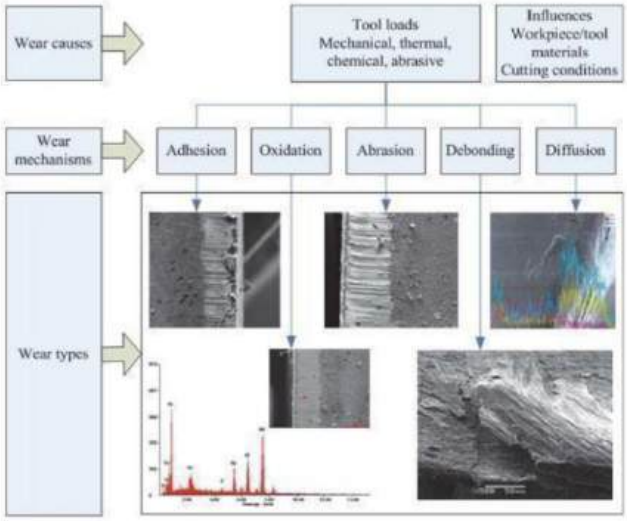

Figure 6: Schematic diagram of wear causes, mechanism, and types in nickel based super alloys cutting [40]

— **Adhesive wear:** This form of wear occurs usually due to the flow of the work piece material at high temperature and pressure enabling the formation of the built-up edge (BUE). The unstable built-up edge or layer sticks to the flank face or rake face of the tool and will eventually get damaged. During this process, the workpiece material and residual chips are continuously getting removed due to a work hardening effect. The tool gets damaged when the adhered material from the tool surface is peeled off due to the removal of the built-up edge (BUE). The cutting temperature at low cutting speed is relatively low which makes it difficult

for the tool and the work piece material to plastically deform. On the other hand, the cutting temperature is relatively very high at higher cutting speed favoring the conditions of chemical and diffusion wear. As a result, the moderate speed of machining still favors the high temperature circumstances which are helpful for the adhesive wear.

Li et al [41] performed cutting tests of the Inconel 718 with CVD and PVD coated carbide tools and observed different wear mechanism while using the ceramic cutting tools. They found that wear of the cutting edge was not significant however, the coating peeled off and adhesion phenomenon was mainly on the cutting edge. When they tried to cut Inconel 718 with ceramic SiAlON tool and, tool chipping was noticed. The increase in cutting speed (240 m/min to 300 m/min) has shown profound changes to the flank and nose concerning the adhesive wear. Furthermore, a further increase in cutting speed and feed rate has depicted cracks on the rake face and at some points even breakage as well.

Hao et al. [42] performed the turning of Inconel 718 with PVD TiAlN coated carbide tools and found that when the cutting speeds are low as of the value 20 m/min, the adherence and accumulation of the work piece material on tool surface is noticeable in form of built-up edge (BUE). The built-up edge was not stable enough and keep on removing with the flow of chips as the process of machining progressing leading towards the chipping and spallation of the tool-material complemented through very small cracks on tool surface as shown in Figure 7. Nonetheless, an increase in the cutting speed [28] increases the temperature which eventually will soften the workpiece material conducive to quickly adhere to the tool and as a result, the adhered area expands on the tool surface. Liu et al. [43] proposed that under very high temperature and pressure conditions, the plastic deformation of the rake face has been confirmed showing formation of a new surface where atoms from the tool and workpiece material surface absorb in such a way that they form an absorption point. The relative movement of the workpiece and tool breaks the adhesion point resulting in shearing of the gain group by the other side. Wang et al [44] conducted a study with coated carbide tools and witnessed that employing the PVD TiAlN or TiN coating on the carbide tools can have considerable reduction in chipping phenomenon. Zhu et al [45] analyzed the cBN tool wear mechanism against nickel based alloys and observed diffusion and adhesion as the prominent wear mechanisms.

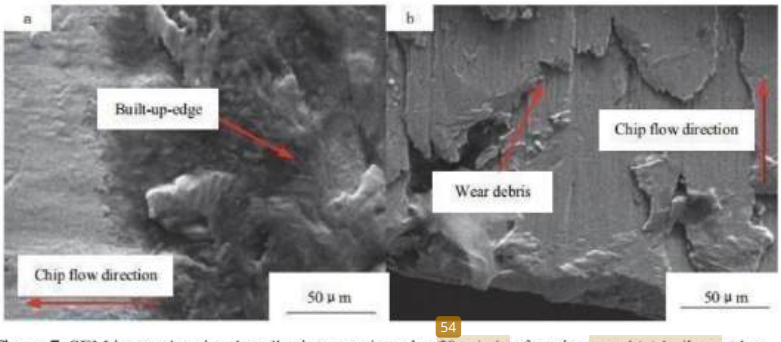

Figure 7: SEM image showing the adhesive wear in tool at 20 m/min of cutting speed (a) built-up edge (b) wear-debris [42]

— **Abrasive wear:** Scientific studies have disclosed that the friction phenomenon between the hard particles of carbides present in nickel based super alloys and the flaking off coating or carbide particles from the tool matrix are the primary reason behind the abrasive wear when machining of nickel based super alloys is performed with different tool materials. It has also been observed that when machining is performed, the material tends to flow on both sides of the tool and due to the hardening effect, it leaves burrs on the surface of the tool which are contributing to the abrasive wear. The presence of the deep grooves on the tool rake and flank face are a mark of the abrasive wear as well as the notch depth at the point of contact between workpiece and tool material [46-48].

Ezugwu et al. [49] investigated ceramic tools for machining of nickel based alloys and proposed that ceramic tools have shown good stability in their hardness at high temperatures and abrasive wear has been depicted as the main wear mechanism. The wear happened due to the shredding of fine carbide particles between the workpiece chips and tool material under extreme pressure accompanied by the increased strength of workpiece material due to hardening effect during the machining process. They pointed out that low cutting speed increases the built-up edge while at medium speed, it softens the built-up edge and its height get decreased. However, high cutting forces renders the tool cutting edge to collapse resulting in fracture of the tool cutting edge [43].

While drilling the Inconel 718, Chen et al. [50] proposed that carbide tools coated with TiAlN have undergone primarily abrasive wear mechanism. Similarly, Olufayo et al. [51] conducted drilling test study on nickel based super alloy Rene 65, and described flank wear as the primarily occurring wear phenomenon due to high value of abrasive forces enabled by the corrosion at the tool cutting edge. Moreover, Deng et al. [52] used Al_2O_3 ceramic tool reinforced by SiCW particles and TiB_2 particles, and noticed the formation of the grooves in the sliding direction of the workpiece and tool material indicating the flank wear on the tools surface. They also proposed that abrasive wear was caused by the frictional force between the falling off hard debris, tool, and hard particles present in the workpiece material.

— **Other wear mechanisms:**

Apart from the adhesion and abrasive wear, diffusion wear is another commonly occurring wear mechanism during the machining of super alloys due to the high temperature. The very high temperature at the tangent point of workpiece and tool material, e.g. during high speed cutting, both the workpiece and the tool material are activated and tend to diffuse into each other leading to the diffusion wear [49]. Zhu et al. [40] analyzed during cutting of nickel based super alloys that high cutting temperature is an ideal environment for the close contact of the tool, workpiece, and chip for diffusion of atoms via the interface of the chip. Therefore, for the cemented carbide tools, cobalt (Co) is highly likely to be lost through diffusion, thus, the cobalt content presence in the cemented carbide tools can give an indication about the diffusion wear. Kasim et al. [53] has reported that tool performance of the carbide tools during machining of Inconel 718 has been limited by the diffusion wear. On the other hand, for the ceramic tools with high cutting speed, an increase in temperature has been noticed. Under high pressure and temperature, it is very likely for the diffusion wear to occur. This notion has been fortified by Ezugwu et al. [54] that it is highly possible that diffusive wear will occur on the smooth surfaces probably due to the fact that when cutting of the Inconel 718 is performed with help of ceramic tools, not only elements of the workpiece and tool material got transferred on surfaces but can also damage the tool by penetrating into its surface.

Chemical wear is another form of the most frequently occurring wear at the contact area of the workpiece and tool material. The tool material is prone to chemical reaction with the surrounding environment such as air (in case of dry machining) or cutting fluid, oxidizing the tool surface leading to impurities generation followed by the bond looseness in the tool and eventually causing an irreparable damage to the surface of tool [55]. Chemical wear is mostly noticed at high or extremely high temperature, as at low temperature, the tool material has quite stable interatomic structure which is not easy to destroy [49]. The chemical reaction of the tool material with surrounding environment decreases its strength by softening and also reduces its hardness thereby opening the channel for excessive damage through other wear mechanisms. Pawade et al. [56] used the PCBN tools (uncoated generic and TiN coated) for high speed turning of Inconel 718 (HRC 45), and dense craters has been observed as the leading cause of the tool failure at 250-350 m/min of cutting speed. The chemical wear resulting from the chemical reaction of the abrasive wear particles on the surface of tool has been noted as the cardinal wear mechanism. As cBN tools has special chemical attraction for Ni, Fe, Cr, and Nb elements, so when high speed cutting is performed at high temperature, cBN tool material coating is damaged.

Stainless Steel machining also poses various challenges for the tools as being reported by various scientific studies. For example, Diniz et al. [57] conducted turning experiments with cemented carbide tool material having grade ISO P15 (coated with TiCN, TiN, and Al_2O_3 triple layer) for AISI 1045 steel. The observations have revealed that the rake face had the adhered material on its surface with very shallow crater wear owing to the protection given by chemically stable triple

layer coating. However, the flank wear was caused by the attrition and abrasion without taking into consideration the cutting speed. Likewise, Rosa et al. [58] performed drilling of AISI 1548 steel with PVD coated cemented carbide drill, and proposed that the primary wear mechanism has been seen as the attrition wear. The hard particles generated from the attrition wear serves as the source of abrasive wear to damage the tool concomitantly. The presence of the parallel ridges confirms the mechanism of abrasive wear. Through their experimental study with different tool substrate material, Rosa et al. [58] confirmed the flank wear from the attrition and abrasive wear.

Super duplex stainless steel turning studies by Oliveira et al. [59] with physical vapor deposition coated (TiN and TiAlN) cemented carbide tools has demonstrated flank wear and notch wear (present at the end of depth of cut) the main tool wear mechanism with the later one responsible for ending the tool life. Moreover, Braghini Junior et al. [60] tested the tool life of carbide inserts (ISO grade M20-M40) of tungsten carbide cobalt (WC-Co) substrate coated with TiAlN coating during dry milling of martensitic stainless steel. They found out that the flank wear due to abrasion, and adhesion of the workpiece material on the tool flank surface as shown in Figure 8, was the dominant wear mechanisms. Attrition wear has been depicted as the main wear mechanism with dry milling and mechanical fatigue led to the failure of the tool cutting edge.

In simple words, it has been stated that ductile materials like steel (before tempering and quenching), and stainless-steel show attrition wear as the main wear mechanism. However, the high rate of work hardening creates hard burrs on the end of depth of cut resulting in furrowing effect conducive for removing the coating. As a result, this removal of coating layers promotes the attrition wear which also facilitates the notch wear.

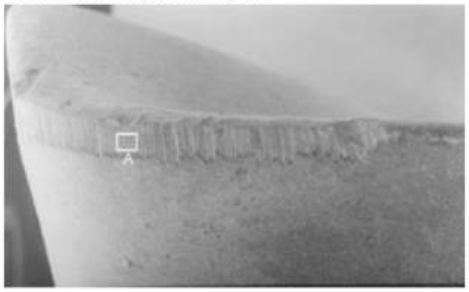

Figure 8: Abrasive wear along the cutting edge during dry milling of PH martensitic stainless steels [60]

Types of Tool Wear:

The above-mentioned wear mechanisms give rise to some certain type of wear characteristics and feature to the tool surface during the machining process which are termed as wear types. As wear mechanism has specific description, wear types also have a number of denotations to explain the wear types in machining tools. These wear types have a common feature used to categorize them

on account of their ability to change the tool geometrical accuracy. Below, the most commonly occurring wear types during machining of stainless steel and nickel based alloys can be found.

— **Flank wear:** It is found on the clearance side of the cutting tool inserts, critically affecting the quality of the cutting process. Workpiece surface finish highly correlates with the flank wear as experimental studies has shown a decrease in surface finish with increase in flank wear. It is impossible to avoid flank wear in cutting process, in fact is the desired wear type as it is predictable, hence allowing insert change in a controlled manner. From experimental analysis, it has been revealed that harder material results in less flank wear being compensated by other wear types such as chemical or chipping as it is highly likely to occur depending on the cutting parameters, as speed, feed, and depth of cut.

— **Crater wear:** Crater wear or cratering looks like a concave pattern occurring on the rake face near the cutting edge. High temperatures are generated, when the chip are flowing over the insert face, the chemical reaction between the tool and workpiece material results in crater wear. This wear type is commonly found in ductile materials where continuous chips during the machining process are formed. Softer tool material experience high crater wear and materials with low thermal conductivity as for example Nickle base super alloys, however, increasing the hardness can diminish this problem effectively. Similarly, a decrease in this sort of wear can be expected with reduced and controlled speed as well as the feed rate.

— **Built-up edge (BUE):** The built-up edge is the material adherence to the surface of the cutting tool insert which keeps on building during the machining process. This form of tool wear is prevalent in machining of stainless steel, nickel based super alloys, and aluminum. The chemical affinity plays important role for starting the built-up edge and it gets worse later in the machining process in such a way that thick adhered layer of material prevents the actual cutting process and breaks the insert eventually. Adding more heat into the cut, by for example increasing the speed, can reduce it significantly.

— **Notching:** Notch wear of tool occurs whilst the base material is having more hardness as compared to the surface material hardness. Notching is common during machining of nickel based super alloys and stainless steel. Also the stress concentration at the contact zone of the tool and the workpiece material can lead to localized notching. The disruption, small impacts, and inclusion in the form of hard particles in workpiece material can also create notch wear. Selection of a tough carbide grade tool materials and reducing the feed rate can reduce notch wear occurrence.

— **Thermal cracks:** are present in perpendicular direction to cutting edge as the changes in temperature are noticed. These cracks appear when hard materials are machined or when interrupted cutting is performed. Tough tool materials having high resistance to wear could be better choice to prevent thermal cracking.

— **Plastic deformation:** High temperature and increased cutting forces are the leading cause of the plastic deformation of the tools. Softening of the hard metal at the cutting edge can leads to plastic deformation during machining operation. It is associated with machining conditions where local temperature and/or loads are high, as for example, in machining hardened steel or materials with low thermal conductivity which gives intense heat generation. The side effect

of plastic deformation is the intensive heating of the cutting-edge combined with the high cutting pressure compressing the cutting-edge nose. As a result, the area of wear zone increases compromising the control on chip formation and surface finish and in the end, poor tool life. However, thanks to the advances in coatings and carbide alloying helps to reduce this failure mode.

— **Chipping:** Heavy mechanical shocks and vibrations from the interrupted cutting leads to chipping which is a very unpredictable edge failure of the tool. Reducing the feed rate, an increase in cutting speed can serve as beneficial factor to reduce chipping phenomenon. Alternatively, inserts of tough grade with strong cutting edge can be employed to avoid this failure mode [61].

Figure 9 shows different types of the tool wear during machining of heat resistant super alloys.

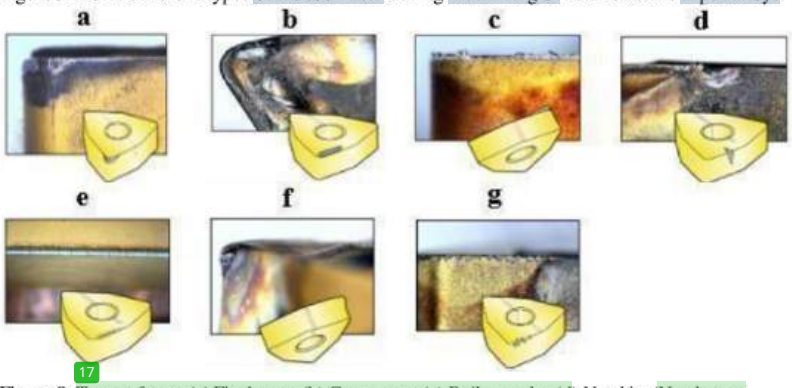

Figure 9: Types of wear (a) Flank wear (b) Crater wear (c) Built-up edge (d) Notching/Notch wear (e) Thermal cracks (f) Plastic deformation (g) Chipping [62]

1.5. High Temperature Tribology

There are various mechanical systems that work at very high temperatures. For example, machines in power plants, hot metal working, machining of super alloys as well as in the aerospace industry. From the perspective of tribology, a system can be thought to operate at high temperature if conventional lubricants are unable to provide lubrication to the operating system. The temperature range for this starts from 300 °C as it is very difficult to withstand against this high temperature for the conventional lubricants (e.g. greases and oils) and they lose their effectiveness by decomposing. Other changes imparted by the high temperature are the variation in mechanical characteristics and enhanced tribo-chemical reactions leading to change in tribological behavior of the contacting surfaces. Due to the challenges and changes imposed by high temperature, it is very important to consider tribology at elevated temperatures [36].

Machining processes are typical examples where high temperature tribology conditions prevails since operating temperatures are over 1000 °C and pressure ranges from MPa to several GPa along

with many hundreds of the m/min sliding speed in a very small localized area of few mm^2 [63, 64]. During the machining process, the effective lifespan of the tool is governed by the high temperature friction and wear mechanism between the tool coating and the workpiece. Typically, these tools are made from the cemented carbide substrate (WC/Co composite) coated with a functional coating to increase the tool robustness and durability. The most commonly used coating is the family of $Ti_{1-x}Al_xN$. This class of coating provides very high wear resistance properties to the tool surface along with superior performance as compared to TiN coating at elevated temperatures [65]. It has been observed that TiAlN coatings enables high speeds and cutting forces resulting from the reduced flank wear. Despite the good performance of TiAlN coatings, there are still challenges and difficulties being faced during the machining of the heat resistant and difficult to machine super alloys with coated tools [66].

The most challenging and tool damaging mechanism is the adhesive material transfer when machining of difficult to machine super alloys such as nickel-based alloy (Inconel 718) and stainless steel (SS 316L) is performed [67, 68]. This is found mostly in the sliding and sticking transition zone and at the rake face of the cutting tool where high temperature conditions are prevailing [69]. The adhesive wear leads to the phenomenon of built-up edge on the edge of the cutting tool and varying the shape of the tool followed by cutting edge breaking. Inconel 718 and stainless steel are materials which promotes the adhesive wear in the tribological contact. In the study conducted by Grzesik et al. [70], they noticed a quite easy adhesive transfer of the material in the dry sliding tribological contact of AISI 304 stainless steel and TiAlN coating. It was observed that surface texturing of the substrate before depositing the TiAlN coating and use of solid lubricant such as MoS_2 proved to be ineffective in preventing the complete transfer of stainless steel on TiAlN coating [71]. However, the change in the adhesive wear behavior of TiAlN coatings with variation in temperature has not yet been explored despite its intensive use in the machining industry. Earlier work conducted by Hardell et al. [72] with ferrous and non-ferrous materials showed a readily occurring transfer of the materials on the TiAlN coatings in sliding test conditions at high temperatures. The reported work also confirmed the presence of the coating constitutes on the opposite/counter surface. Adding more to it, sliding contact of TiAlN PVD coatings with carbon steel demonstrated an easy transfer of carbon steel on the counter coated surface at high temperature as being investigated by Courbon et al. [73]. Moghaddam et al. [74] carried out research on the sliding response of TiAlN coating with stainless steel 316L (SS 316L) and carbide-free bainitic steel at three different temperatures (i.e. 40 °C, 400 °C, and 800 °C). The coefficient of friction (COF) continuously increased with rise in temperature for SS 316L while a decreases in COF with increase in temperature has been noticed for carbide-free bainitic steel. More material transfer for carbide-free bainitic steel at 800 °C was noticed due to its lower strength at high temperature. The formation of a porous oxide layer that acts a solid lubricant and thus reduces the friction coefficient was found in case of the carbide-free bainitic steel. On the other hand, material transfer is of more significance at 40 °C and 400 °C for SS 316L. The formation of aluminium oxide tribo-film helps in reducing the wear of the TiAlN coating.

Similarly, keeping in mind the applications of nickel based super alloys, researchers have tried to explore the tribological characteristics and effect of temperature on the variation of mechanical

properties. Figure 10 shows the variation of specific strength and compressive yield strength of super alloys as a function of temperature.

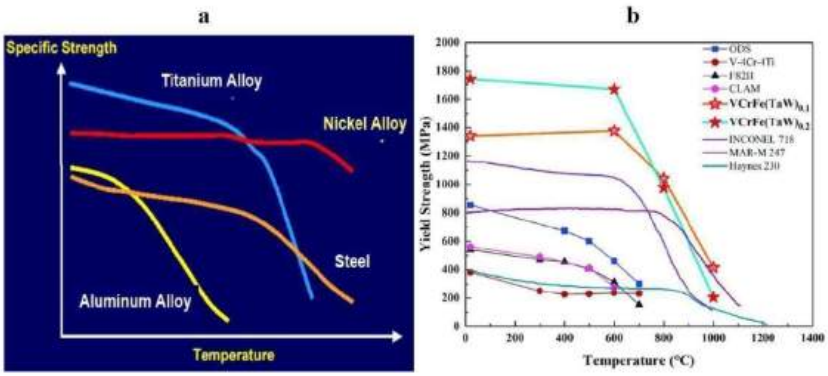

Figure 10: The variation of (a) specific strength [75] and (b) compressive yield strength [76] with temperature for super alloys

The work in literature conducted by Hong et al. [77] about microstructure effect (changed through heat treatment process) on Inconel 690 wear properties states the abrasive wear and plastic deformation as the main wear mechanism. Hardness and grain size effect on Inconel 600 wear properties were analyzed by Li et al. [78]. Their studies depicted a better wear performance with small grain size and high hardness. Some researchers like Xin et al. [79] tried to scrutinize the temperature effect on fretting wear of Inconel 600. The examination through perusal analysis confirmed the presence of less and short length cracks at elevated temperature in comparison to room temperature. Similar experimental research was carried out by Zhang et al. [80] on Incoloy 800 concerning its fretting properties at different temperatures. The results indicated the abrasive wear, delamination, and oxidation as the primary wear mechanism. Dry sliding wear properties for boronized Inconel 718 and untreated Inconel 718 through a ball-on-disk tribo-meter were examined by Gunen et al. [81] at three different temperatures (i.e. 25 °C, 400 °C, and 700 °C). Wear was caused by two-body abrasive wear for untreated Inconel 718. On the other hand spalling and micro-cracking from three-body abrasion was highlighted as the cardinal wear mechanism. Kurzynowski et al. [82] made an attempt to study the tribological characteristics of Inconel 718 in comparison to laser surface alloying employed on Inconel 718. The findings showed an increase in wear resistance index for 28 wt% rhenium (Re) layer applied on Inconel 718 in contrast to Inconel 718 substrate. Moreover, a recent study by Zhibiao et al. [83] on tribological response of Inconel 718 against silicon nitride (Si_3N_4) ball as function of applied load and test duration has been carried out at constant temperature of 300 °C. The results proposed by them indicated the oxidation, abrasion, adhesion and peeling as the main wear mechanism. Longer test duration has increased the material wear and initial wear was more severe for 5 N of load in comparison to 3 N of applied load.

1.6. Existing research gaps

The literature review pertaining to machining of super alloys and the problems which heat resistant super alloys poses to tool performance and surface integrity dictate a great significance of how important it is to select an adequate tool material as well as coating. From the tribological point of view, higher temperatures are an integral part of the machining process and its effect on tool degradation has not received great attention so far. Therefore, it is of extreme importance to understand the high temperature tribology keeping in view the current requirements of the manufacturing industry.

From a fundamental point of view in machining and high temperature tribology, it is apparent that there is a scarcity of in-depth study and analysis of the machining tool and workpiece interaction albeit some researchers have pointed out their findings and observed behavior of materials against multiple coated tools. Therefore, a thorough understanding of the friction and wear mechanism is of utmost importance. Control on the friction level and minimizing the wear of the materials is pivotal to ensure the productivity and quality of end product in machining. The coefficient of friction (COF) governs the heat generation while the tool surface state decides the final surface finish and quality of the product as it controls the shape, geometry, and overall effectiveness of the machining process. High wear and friction not only affects the dimensional tolerances but also the overall productivity of the machining process.

Recent scientific advances have witnessed the developments of various coatings on tool substrate to protect the tool during the machining process. Since the TiAlN coating family is widely used as protective layer on tool substrate, research studies have confirmed the adhesive wear leading to transfer of material and coating damage during the machining process as well as the sliding contact conditions.

There is no scientific investigation which has been performed to analyze the effect of temperature on the adhesive wear of Inconel 718 and stainless steel 316L against TiAlN coating at elevated temperatures. Especially the initial material transfer mechanism for the TiAlN PVD coated surface as well as the initiation mechanism which damages the coating at very high temperatures is not understood. Thus, the current knowledge about the initial material transfer mechanism is inadequate to resolve the problem of adhesive wear, so, it is important to discern the effect of change in temperature on adhesive wear leading to detrimental material transfer. Therefore, this thesis has made a novel attempt to delve deep into understanding the initial material transfer mechanism and create new knowledge on TiAlN (i.e. $Ti_{60}Al_{40}N$ and $Ti_{40}Al_{60}N$) coating damage initiation mechanism during the interaction of difficult to machine super alloys which in our investigations are Inconel 718 and stainless steel 316L (SS 316L) at elevated temperatures.

Chapter 2

2. Aims and Objectives

It can be seen from the discussion in section 1.6 that it is very important to understand the high temperature tribological interaction between the coated tool material and the difficult to machine super alloys. A clear understanding about adhesive wear is missing from the literature related to high temperature interaction of the TiAlN (i.e. $Ti_{60}Al_{40}N$ and $Ti_{40}Al_{60}N$) coated tools and Inconel 718 and stainless steel 316L. Thus, new knowledge accounting for the friction and wear mechanism with different material pairs at high temperature has been created herein to bridge the earlier indicated research gap in scientific research and studies.

The main aim of this work is to build an understanding of the initial (early stage) tribological interaction between the coated tool material and workpiece (difficult to machine super alloys) in sliding wear test.

The specific objectives of the work are:

1) Lab-scale experimental investigation of the friction and wear behaviour at room and higher temperatures for two coating composition and two super alloys
2) To develop a clear understanding of initial material transfer mechanism in sliding test for four pairs involving in the actual machining conditions
3) Characterization of the worn surfaces of Inconel 718 and stainless steel 316L (SS 316L) paired with ($Ti_{60}Al_{40}N$ and $Ti_{40}Al_{60}N$)
4) To find out the best coating and material pair from the high temperature tribology point of view

2.1. Limitations

This work presents the first study of its kind for initial material transfer mechanism for two compositions of coatings against two super alloys at elevated temperature. The tribological process and wear mechanisms are highly complicated and the scope of this thesis has not been able to address all of that issues.

The lab-scale work has been performed under simple conditions and precisely controlled environment which might not be possible to directly transfer to actual machining conditions. As a result, the applicability and translation of the results may not be as straightforward in the actual machining process due to the complex process involved in actual machining operations.

Moreover, the friction and wear data is specific to some pair of materials obtained from the company. Therefore, due to the proprietary nature of the coating deposition and product information, it is not possible to provide the information about the sample process parameters.

Chapter 3

3. Experimental work

The following section explains the material pairs used in the tribological test, the experimental equipment and procedures, and analysis techniques.

3.1. Experimental materials and specimens

3.1.1. Materials

Inconel 718 is used as one of the workpiece materials (in the form of pin) with nominal chemical composition in wt% shown in Table 2.

Table 2: The nominal chemical composition of Inconel 718 super alloy in wt% [83]

C	Cr	Ni	Mo	Al	Ti	(Nb+Ta)	Fe
0.02-0.08	17-21	50-55	2.80-3.30	0.40-0.60	0.90-1.15	5-5.50	Balance

The mechanical properties of Inconel 718 are given in Table 3. The presence of 21% of Chromium enhances the hardness of Inconel 718 significantly.

Table 3: Mechanical properties of Inconel 718 [84]

Elastic modulus E (GPa)	Thermal conductivity K ($Wm^{-1}K^{-1}$)	Tensile strength σ_b (MPa)	Yield strength σ_s (MPa)	Hardness H (HV)	Melting temperature (°C)	Density (g/cc)
204	11.4	1375	1100	460.5	1336	8.17

The other employed difficult to machine material is the stainless steel 316L (in the shape of pin) having nominal chemical composition in wt% depicted in Table 4.

Table 4: Nominal chemical composition of Stainless Steel 316L (SS 316L) [74]

C	Si	Mn	Cr	Mo	Ni	P	Fe
≤ 0.03	≤ 0.75	≤ 2.0	16.5	2.1	11	0.045	Balance

The mechanical properties of stainless steel 316L are listed in Table 5.

Table 5: Mechanical properties of Stainless Steel 316L [85]

Elastic modulus E (GPa)	Thermal conductivity K ($Wm^{-1}K^{-1}$)	Tensile strength σ_b (MPa)	Yield strength σ_s (MPa)	Hardness H (HV)	Melting temperature (°C)	Density (g/cc)
193	14.0 - 15.9	485	170	175±14	1375 - 1400	8

A cemented carbide (WC/Co) substrate coated with two different PVD-TiAlN coatings has been used as the counter material in the form of disc. The chemical compositions of the used TiAlN coatings are $Ti_{60}Al_{40}N$ and $Ti_{40}Al_{60}N$.

3.1.2. Test specimens

In this experimental work, a hemispherical pin made of the workpiece materials (i.e. Inconel 718 and stainless steel 316L) has been employed as the upper specimen. The actual geometry and shape of pin is like a cylinder with one end having a spherical shape. The spherical shape side of the pin has 5 mm tip radius with other side consisting of 10 mm diameter of cylinder. The nominal length of the pin is 10 mm. The Inconel 718 pins have an arithmetic surface roughness (Sa) of 0.825±0.276 µm and whereas stainless steel 316L demonstrates value of 0.722±0.124 µm based on 18 sample surface roughness measurement for each material shown in Figure 11.

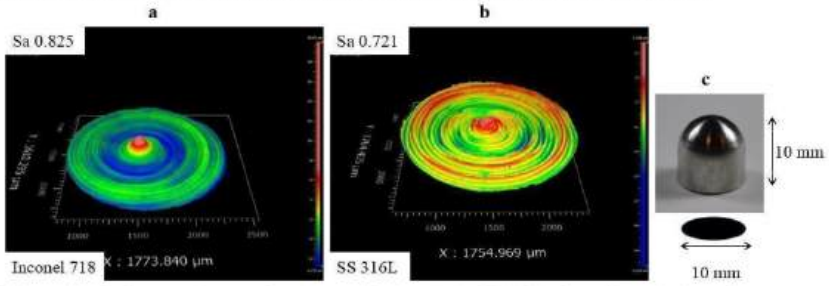

Figure 11: Surface roughness of (a) Inconel 718 and (b) SS 316L from 3D optical profilometer (c) photograph of pin specimen

A square disc with 12.65 mm x 12.65 mm dimensions and flat surface was used as the lower specimen. The thickness of the disc is 4.75 mm and it is made of cemented carbide (WC/Co) acting as substrate material coated with a 2.6 µm thick TiAlN coating (two variations i.e. $Ti_{60}Al_{40}N$ and $Ti_{40}Al_{60}N$) with help of cathodic arc evaporation (Arc-PVD). A Vickers Hardness (HV) test with load of 300 g has been performed to measure the hardness value of both coatings. The $Ti_{60}Al_{40}N$ coated disc has hardness of 2013±117 while $Ti_{40}Al_{60}N$ has 1922±133. The arithmetic surface roughness (Sa) of $Ti_{60}Al_{40}N$ coated disc is 0.156±0.006 µm and for $Ti_{40}Al_{60}N$ is almost the same with more standard deviation i.e. 0.154±0.015 µm, as revealed in Figure 12.

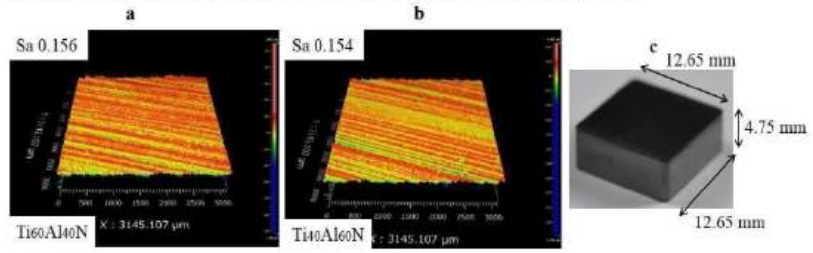

Figure 12: Surface roughness of (a) $Ti_{60}Al_{40}N$ coating (b) $Ti_{40}Al_{60}N$ coating and (c) photograph of disc specimen

There are four pairs for the tribological tests at elevated temperatures. Table 6 presents the combinations of different materials in the form of upper and lower specimen for tribological test.

Table 6: The tribological test pairs in the form of upper and lower test specimens

Tribological test pairs		
	Upper specimen	**Lower specimen (coated disc)**
Pair 1	Inconel 718	$Ti_{60}Al_{40}N$
Pair 2	Stainless steel 316L (SS 316L)	$Ti_{60}Al_{40}N$
Pair 3	Inconel 718	$Ti_{40}Al_{60}N$
Pair 4	Stainless steel 316L (SS 316L)	$Ti_{40}Al_{60}N$

3.2. Optimol SRV-3 tribological test configuration

The Optimol SRV reciprocation friction and wear tester uses an electromagnetic drive system to operate a sliding tribological test. An upper specimen mounted on the upper holder under normal load oscillates back and forth in the range of input stroke length against the lower stationary disc. The normal load is applied through servo motor and spring deflection mechanism. A wide variety in range of the SRV temperature is achieved via a cartridge heater. The lower specimen is placed on the cartridge heater enabling it to achieve different surface temperatures depending on the test conditions and requirements. Moreover, the test parameters are controlled with the help of a computerized control system according to specific conditions. Furthermore, the data for the friction, temperature, frequency, and applied load is obtained continuously from the data acquisition system on the computer screen [86]. An Optimol SRV-3 with operating test configuration shown in Figure 13.

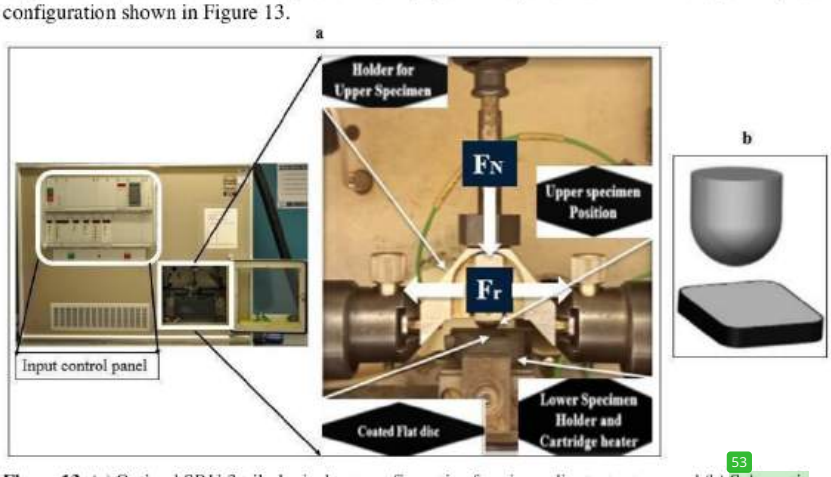

Figure 13: (a) Optimol SRV-3 tribological test configuration for pin on disc test set-up, and (b) Schematic diagram of the pin-on-disc tribological test [74]

3.3. Test methodology

In this study, the test equipment's samples and sample holders employed in the tribological test are first cleaned with acetone, heptane followed by ethanol to remove any contaminants from the surfaces. Then, the test specimens and sample holders are placed in a glass beaker separately and cleaned with the help of heptane in an ultrasonic bath whose running time spanned to 480 seconds shown in Figure 14.

Figure 14: Ultrasonic bath for cleaning purpose

Once the ultrasonic bath cleaning is complete, the samples are taken out from the glass beaker and cleaned gently with the help of soft tissue paper in order to dry the sample holder and specimen. The corner and bottom surface of sample holder and specimens were dried with pressurized air. The hemispherical pin is then mounted in the upper specimen holder and the flat coated disc in the lower specimen holder to prepare them for the tribological test as shown in Figure 15.

Figure 15: Pin and coated disc in upper and lower specimen holder respectively

Subsequently, a normal load is applied enabling a point contact between the upper and lower specimen i.e. pin and disc respectively, and wear test starts after 2-3 seconds as soon as the start button is pressed on the control panel of the tribological test machine.

3.4. Test parameters

The tribological test has been performed at the three different temperatures of 40 °C, 400 °C, and 760 °C by keeping in mind the maximum applied temperature limit of 900 °C of the Optimol SRV-reciprocating sliding friction and wear tester. The effective surface temperature is usually less compared to the input temperature in SRV due to the heat losses. For the cemented carbide substrate coated with TiAlN coating, a maximum surface temperature has been determined through spot welding of a thermocouple on the surface of the dummy TiAlN coated cemented carbide sample. A significant difference in test temperature has been used in order to obtain a clear and pronounced transition in frictional behavior and wear mechanism of the tested specimens. A single load of 20 N has been used as the test load with 10 N as the preload to adjust the alignment and prepare the sample pairs for proper point contact. Each test has been performed two times to check the repeatability of the tests. The test parameters are listed in Table 7.

Table 7: Tribological test parameters employed in the tribological tests

Tribological test parameters	
Frequency (Hz)	5
Time (sec)	2
Stroke length (mm)	2
Sliding speed (m/s)	0.02
Surface temperatures (°C)	40, 400 (470 in SRV), and 760 (900 in SRV)
Pre-load (N)	10
Applied load (N)	20

It is important to mention here that apart from the actual tests being reported here, various other tests with different materials and coating composition were performed to find out the suitable frequency at which machine motor produces no noise, stable stroke length, consistency in wear scar length, and actual surface temperature.

3.5. Analysis techniques

In the analysis of the test specimens, different analysis techniques has been employed and discussed as follows:

3.5.1. Nikon D3500 camera

A digital single lens reflex (DSLR) camera (Nikon D3500) has been used to take the images of the upper and lower specimens including the upper and lower specimen holder to have an idea how the specimens look after mounting the holder. The images of the tribological test set up and other instruments used in this study are captured via Nikon camera.

3.5.2. Zygo-9000 3D Optical Profiler

This instrument works on the principle of optical interferometry using the interference fringes to form the 3D images of a surface. Surface analysis mode was used to measure the wear scar and damage on the surfaces of the pins and discs. The linear measure mode allows to measure the length and width of the deposited material on the disc. A shape factor of higher order enabled to achieve a smoother and more coherent 3D surface image of the pins.

The amount of deposited material on the coated disc was obtained by using the Regions mode of the 3D Optical Profiler by applying the form removal command first, then setting up the reference planes followed by the selected regions of test surface and unworn surface. The volume up, down, and net results section calculate the deposited material volume in comparison to the unworn surface. Surface analysis including the surface roughness measured prior to tribological test, deposited material scar length, width, and wear volumes of the pin and disc has been calculated with help of Zygo-9000 3D Optical Profiler. The 3D Optical Profiler with its software is shown in Figure 16.

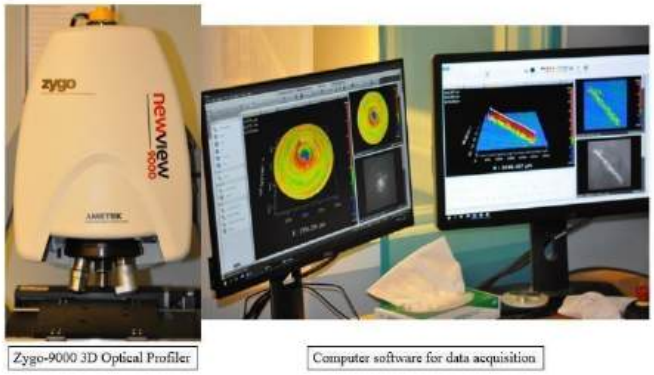

Figure 16: Zygo-9000 3D Optical Profiler

3.5.3. Jeol JCM-6000 PLUS: Scanning Electron Microscopy (SEM)

Scanning electron microscope working on the principle of the electron interaction from the electron gun and the surface of the materials to produce a magnified image of the surface. These electrons from the electron gun travel in vacuum vertically to reach the material surface. It is usually accompanied with two analysis mode, i.e. back scattered electrons (BSE) used to find out the compositional information, and secondary electron imaging (SEI) for obtaining the surface topographical information.

The secondary electron imaging (SEI) mode combined with high probe current (high PC) feature of Jeol JCM-6000 PLUS SEM has been utilized to get a clear and high-resolution images of the adhered material and characterize the surface to find out the wear mechanism.

3.5.3. Energy Dispersive X-ray Spectroscopy (EDS)

The energy dispersive x-ray spectroscopy is an analytical technique usually works in conjunction with SEM to analyse the elemental composition of the surface and chemical analysis of the specimen. In this study, EDS has been used to confirm the presence of the adhered or transferred material as well as the rupture of the coatings from the TiAlN coated discs. Figure 17 shows the Jeol JCM-6000 PLUS SEM/EDS used in this study.

Figure 17: Jeol JCM-6000 PLUS SEM/EDS

3.5.4. Digital weighing balance

A digital weighing balance with precision of 0.01 mg and maximum range of 220 mg weight measuring capacity was used to determine the mass loss of the test specimens exhibited in Figure 18. The measurement of mass loss from the digital weighing balance were converted to volume loss by using the density of the pin materials and has been counter checked with the volumetric gain and loss from the Zygo-9000 3D Optical Profiler.

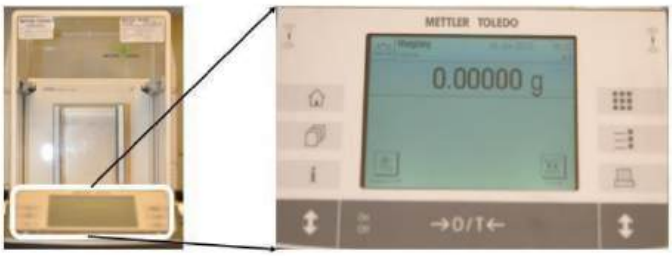

Figure 18: Digital weighing balance

3.5.5. Data analysis from the tribological tests

The data in the tribological test for example, frequency, temperature, sliding speed along with the test duration were closely monitored for each test. Also, the stroke length and frequency of oscillation data was used to find out the sliding velocity. Then, the coefficient of friction (COF) curves obtained from the data analysis section of the SRV programed software to make frictional behavior comparison of different pin materials and coating composition. In the end, the average coefficient of friction in the stable region has been calculated from the friction data.

Chapter 4

4. Results and discussion

$Ti_{60}Al_{40}N$ coated disc against Inconel 718 and Stainless Steel 316L

4.1. Effect of temperature on friction (COF)

This section deals with the tribological behavior of Inconel 718 and stainless steel 316L paired with $Ti_{60}Al_{40}N$ in a pin on disc test set-up. The evolution of the coefficient of friction (COF) with time for Inconel 718 and SS 316L in sliding test against $Ti_{60}Al_{40}N$ coating is shown in Figure 19. It can be seen that Inconel 718 COF values increases with increasing temperature from 40 °C to 400 °C, however a decrease in COF value at 760 °C has been observed. The running-in period for the Inconel 718 at the room temperature is around 1.75 seconds whereas at higher temperature of 760 °C, it span to 2 seconds. On the other hand, stainless steel 316L (SS 316L) showed a continuous increase in the friction value with rise in temperature. The steady state running-in period has a higher discrepancy at the 40 °C and 760 °C. A perusal analysis of the graph depicts that at higher temperature, the instability in the running-in periods gives increase and drop in friction value. The behavior can be attributed to the more deformation of the pin materials until the steady state is achieved at 760 °C. Alternatively, the material can have the lower bulk strength at higher temperatures [87].

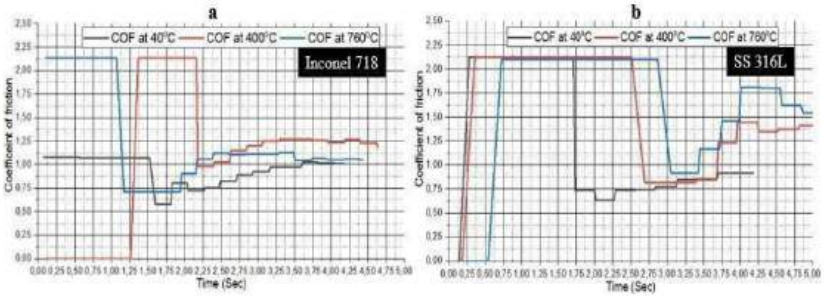

Figure 19: The evolution of COF at 40 °C, 400°C, and 760°C for (a) Inconel 718 (b) Stainless steel 316L, in a sliding wear test against $Ti_{60}Al_{40}N$ coated disc

The steady state average coefficient of friction with error bars showing standard deviation for Inconel 718 and SS 316L are given in Figure 20. The graph demonstrate that Inconel 718 and SS 316L response towards $Ti_{60}Al_{40}N$ coating shows a radical difference. The room temperature (i.e. 40 °C) COF values for both material are very close to each other. Contrary to it, at 760 °C the values are drastically different with opposite trend. The overall trend for both of materials is quite similar with less increment in friction value for Inconel 718 in comparison to SS 316L.

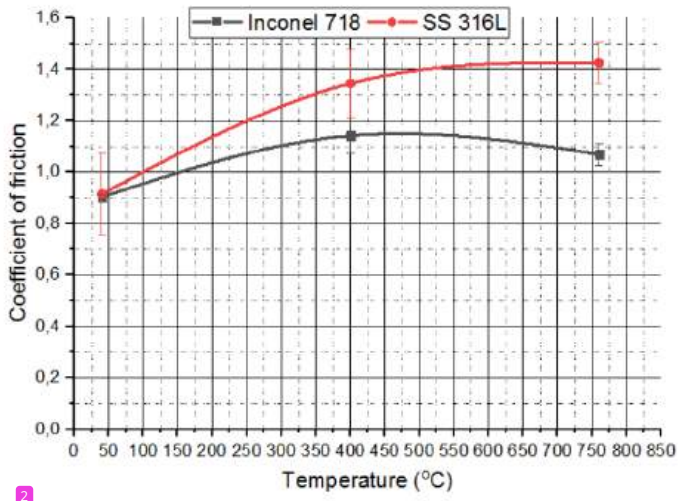

Figure 20: The average steady state coefficient of friction for Inconel 718 and SS 316L during sliding wear against $Ti_{60}Al_{40}N$

4.2. Effect of temperature on wear

The volumetric loss and gain with standard deviation as error bars for Inconel 718 and SS 316L pins in a sliding wear test against $Ti_{60}Al_{40}N$ coated disc at three different temperatures is shown in Figure 21. The negative values shows the volume loss of the pin specimens as a result of wear calculated with the help of the digital weighting balance by taking 5 measurements of each specimen before and after the test to obtain the average volume before and after the tribological test. A detailed look at the results shows that temperature had a profound effect on the wear of the workpiece materials (pins). The volume loss is quite high for Inconel 718 at room temperature of 40 °C probably resulting from the high surface roughness and mechanical deformation generated from the interaction of asperities on pin and surface irregularities on the disc surface. However, an increase in temperature renders the Inconel 718 specimen to undergo plastic deformation followed by strain hardening and reduced volume loss at elevated temperature [82]. Contrary to this, very negligible material transfer on the coated disc observed which showed an increasing trend until 760 °C where highest volume of material transfer noticed.

For SS 316L, the volume loss for the pin is very small and increased with increase in temperature at 400 °C. The volume loss at 400 °C can be ascribed to the low bulk hardness of the SS 316L at high temperatures. A slight reduction in wear volume at higher temperatures coming from the formation of oxides and tribo-film, thereby smoothing the surface and reducing the SS 316L pins volume loss [88]. The coated disc wear volume measurements showed a pronounced increase in transferred material with rise in temperature. At 760 °C, the transferred material is higher for SS

316L as compared to the Inconel 718 pair which can be attributed to the low strength of the SS 316L at higher temperature.

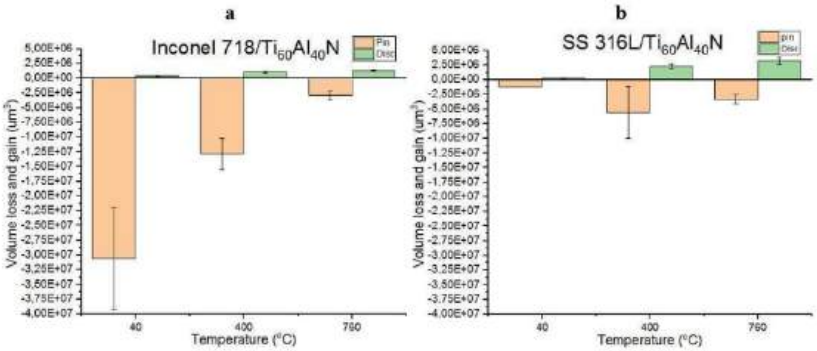

Figure 21: Volumetric loss and gain for Inconel 718 and SS 316L against $Ti_{60}Al_{40}N$

4.3. Worn surface analysis of Inconel 718 against $Ti_{60}Al_{40}N$ coating

In order to obtain a clearer picture and in-depth insights about the active wear mechanism at higher temperatures, the tested specimens' worn surfaces are characterized with Zygo-9000 3D Optical Profiler to investigate the surface topography complemented with SEM and EDS analysis of the Inconel 718 pins and $Ti_{60}Al_{40}N$ coated disc in Figure 22 and 23 respectively.

The surface analysis of the worn surface of coated disc reveals the material transfer and adhesion leading to built-up material in the form of patches at 400 °C and 760 °C. Additionally, there is a very negligible transfer of the material at 40 °C which can be a result of the pure mechanical interaction of the surface irregularities on the disc surface and asperities present on Inconel 718 pin. The pin specimens shows the formation of scratches and grooves resulting from interaction with the transferred material on the $Ti_{60}Al_{40}N$ coated disc. The high concentration of the material accumulation on the edges of the pin signs towards the prevalence of the excessive plastic deformation at elevated temperatures.

Furthermore, the worn surfaces on the coated disc depicts the transferred material accumulation on the edges at 400 °C while material is transferred uniformly on the disc at 760 °C. Conversely, Inconel 718 pins manifest more deep grooves formation and excessively damaged surface at 760 °C confirmed by the Zygo images in Figure 22. However, the worn pin surfaces at 40 °C and 400 °C looks pretty similar with more deformed surface at 400 °C. The transferred material area got enhanced with rise in temperature on coated disc which is perfectly in line with the volumetric gain of the transferred material on the coated disc as mentioned in Figure 21.

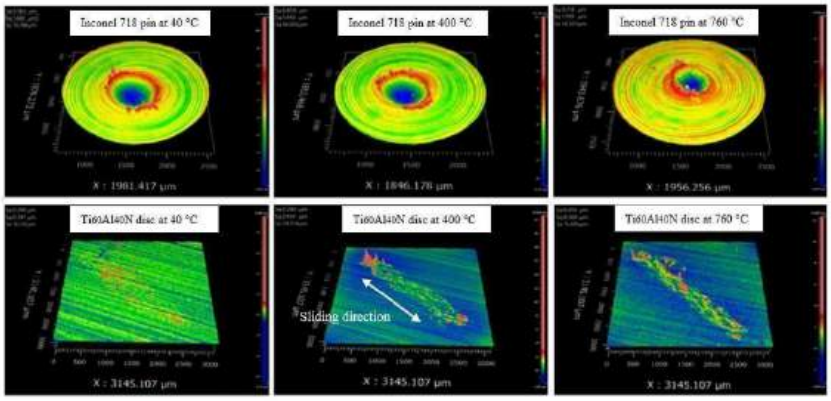

Figure 22: The worn surface topography images for the Inconel 718 and $Ti_{60}Al_{40}N$ coating at 40 °C, 400 °C and 760 °C

A detailed look at the SEM of Inconel 718 at 400 °C shows that the surface was smoothened with rise in temperature under plastic deformation due to the combined action of shear and compressive sliding movement under the load. This smoothening of the pin surface is more significant at elevated temperature of 760 °C which might be resulting from the oxides formation. These oxides prevent the direct contact of the material surfaces.

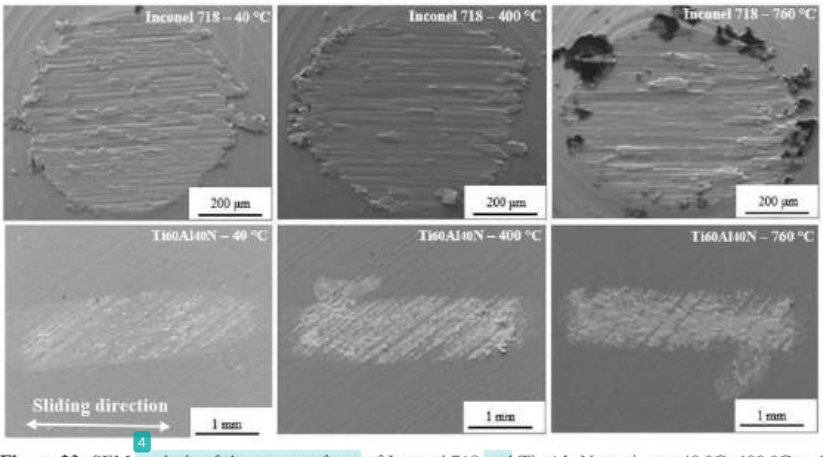

Figure 23: SEM analysis of the worn surfaces of Inconel 718 and $Ti_{60}Al_{40}N$ coating at 40 °C, 400 °C and 760 °C

Figure 24 shows details of the built-up material on the coated disc at 400 °C in the form of patches and islands of the transferred material. The transferred material is not distributed uniformly but along the surface irregularities on the disc. This implies that mechanical initiation is a contribution to the initiation of material transfer. The height of the built-up material is more at the edges in a range of microns. Large chunks of material found as shown in Figure 24 (b). The surface disintegration enabled by the compressive shear load creates small particles on the surface.

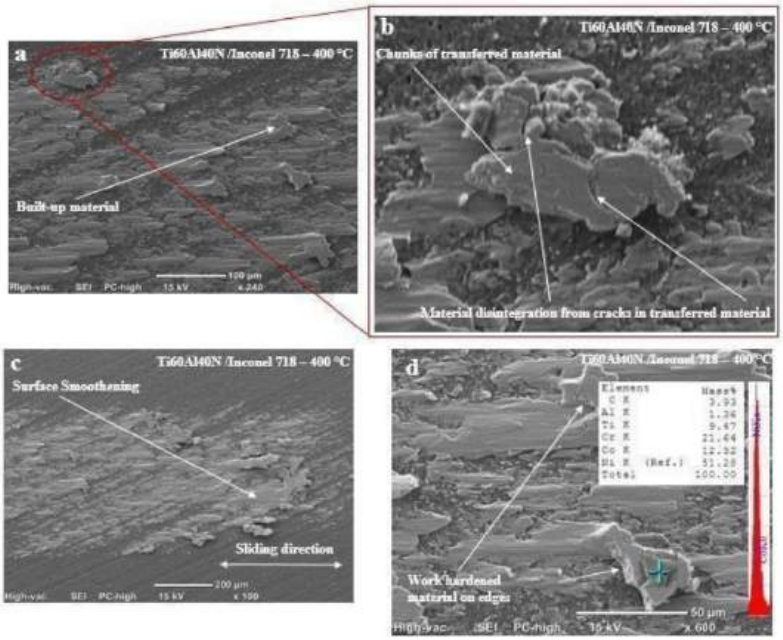

Figure 24: SEM and EDS analysis of transferred material on the $Ti_{60}Al_{40}N$ coating tested against Inconel 718 at 400°C

At 760 °C as shown in Figure 25, the surface got oxidized as confirmed by the EDS spectrum and also the mapped area of Figure 25 (b). This oxide formation can give rise to oxides layer on the built-up material acting as a solid lubricant that can separate the contact of the original surfaces of the Inconel 718 and $Ti_{60}Al_{40}N$ coating. Eventually, there will be less metal-to-metal contact leading to reduce frictional forces and drop in coefficient of friction value. As a result, it can be postulated that the low coefficient of friction at 760 °C results from the oxides formation combined with reduced yield strength and hence easier deformation [83].

The SEM micrograph also demonstrates the smoothening of the load bearing part of the material transfer on the surface, which is comparatively more to 400 °C test conditions enabled by the high

oxides formation at elevated temperatures. Some grooves and ridges on the built-up material shows signs of abrasion on the surface. Moreover, the surface of the $Ti_{60}Al_{40}N$ coated disc showed no rupture and peeling of the coating at 400 °C and 760 °C confirming that coating surface has not been degraded.

From the SEM analysis at three temperatures, it can be concluded the adhesion is the dominant wear mechanism at 400 °C and 760 °C. However, at room temperature, it exhibits more of mechanical deformation of the surfaces with abrasive action coming from the surface irregularities on the coated disc.

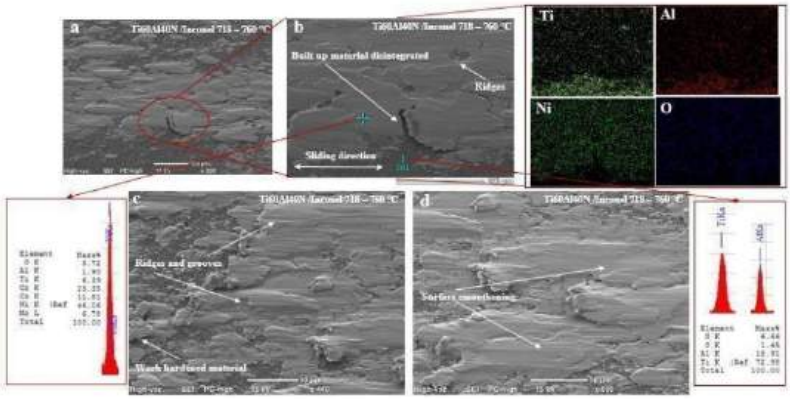

Figure 25: The SEM and EDS mapping of transferred material on the $Ti_{60}Al_{40}N$ coating tested against Inconel 718 at 760°C

4.4. Worn surface analysis of SS 316L against $Ti_{60}Al_{40}N$ coating

The worn stainless steel 316L (SS 316L) pin surface after a wear test against $Ti_{60}Al_{40}N$ coated disc has been characterized and shown in Figure 26 and 27. The surface topographical images reveals marks in the form of thin parallel scratches from the mechanical interaction of the hard coating surface and SS 316L at 40 °C. There is no plastic deformation at room temperature of the SS 316L pin and absence of islands of transferred material was noticed [89].

At 400 °C, the amount of the transferred material increased significantly as a consequence of thermal softening leading to increased adhesion of 316L stainless steel at elevated temperature. This pronounced material transfer at 400 °C was validated by the higher surface roughness of the worn surface compared to 40 °C.

As far as material accumulation of plastically deformed material is concerned on coated disc, 316L stainless steel proclaim it to be higher at 400 °C and 760 °C with more transfer of material at 760 °C due to the thermal softening of SS 316L.

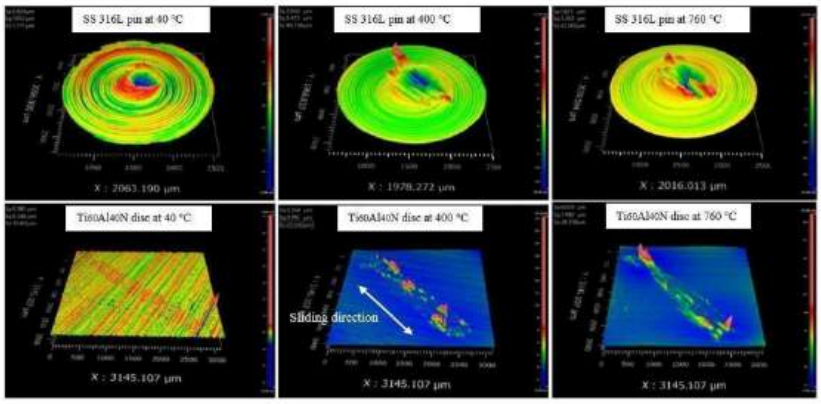

Figure 26: The worn surface topography images for the SS 316L and $Ti_{60}Al_{40}N$ coating at 40 °C, 400 °C and 760 °C

The worn surfaces of pin at 400 °C and 760 °C shows the formation of wide and deep grooves with surface disintegration removing the larger islands of the SS 316L material from center and displacing it to the edges. Therefore, it indicates that transfer of material due to adhesion is the active wear mechanism at 400 °C and 760 °C. An increase in transferred material at 760 °C might be attributed to lower bulk strength of SS 316L as a consequence of thermal softening [90].

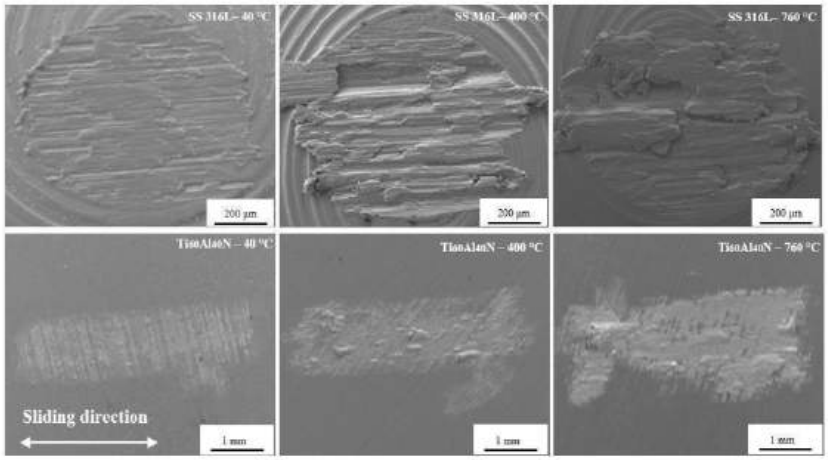

Figure 27: SEM analysis of the worn surfaces of SS 316L and $Ti_{60}Al_{40}N$ coating at 40 °C, 400 °C and 760 °C

A magnified SEM analysis of the coated disc at 400 °C exhibits the formation of smooth surfaces of the built-up material as well as the transferred material surface. This phenomenon can be assigned to the oxidation of the built-up material as shown by the EDS analysis. The high temperature shearing action of the compressive load enable the transferred material to dis-integrate as shown in Figure 28 (c). Alternatively, at elevated temperature of 760 °C, excessive oxidation of the surface takes place which in effect makes the surface smooth. The EDS analysis of the built-up material depicts the presence of oxygen and chromium on the surface of built-up material giving an indication of the presence of chromium oxides on the surface. Chromium oxides are usually harder than the iron oxides and their fracture leading to oxide debris coming in contact of the SS 316L and $Ti_{60}Al_{40}N$ coating during sliding can cause increase in frictional forces. Probably, this is part of the reason behind the increase in coefficient of friction value for SS 316L at 760 °C, combined with increased adhesion at elevated temperatures [74, 90].

It is worth noting here that the grooves in SS 316L pin at 760 °C are finer and in the middle of the contact area as shown in Figure 28 (d) and (e). This can be attributed to some complex oxides formation altering the wear behavior at elevated temperature. The fine and flat region on the SS 316L pin in center including some disruption of the surface might manifest the spalling and delamination of the oxides layers [91].

Figure 28 (f) EDS mapping validate oxidation of the transferred material (iron) occurring at 760 °C. Therefore, it can be inferred from the SEM and EDS analysis that adhesion is the main wear mechanism at 400 °C while the combined action of oxidative wear and adhesion are responsible for wear at higher temperature (i.e. 760 °C).

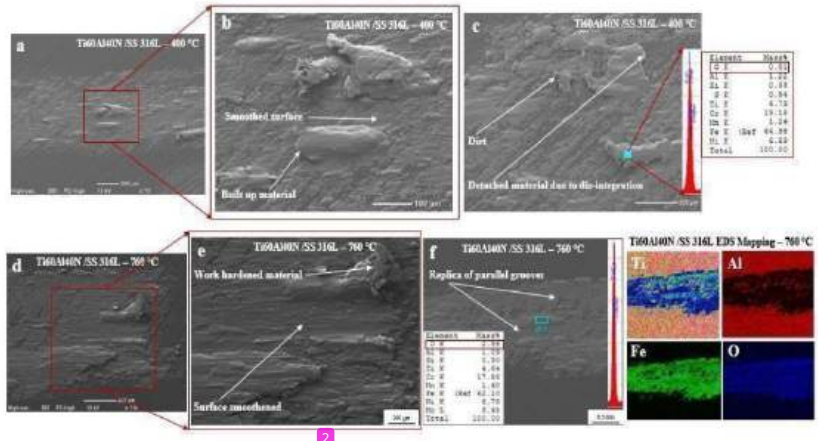

Figure 16 The SEM and EDS mapping of transferred material on the $Ti_{60}Al_{40}N$ coating tested against SS 316L : (a), (b) and (c) at 400 °C; and (d), (e) and (f) at 760 °C.

$Ti_{40}Al_{60}N$ coated disc against Inconel 718 and Stainless Steel 316L

This section of the experimental study has paid attention to the change in friction and wear behavior by varying the composition of the coating. A detailed discussion of the observed findings and results have been provided below:

4.5. Effect of temperature on friction (COF)

Figure 29 shows the evolution of the coefficient of friction with time for Inconel 718 and stainless steel 316L at three different temperatures. A careful analysis shows that Inconel 718 friction response increases with rise in temperature until 400 °C. At higher temperature, the coefficient of friction (COF) falls down significantly in such a way that its value decreases below the COF value at 40 °C. A closer look at the COF value at 40 °C manifest the continuous rise in friction value which can be ascribed to the pure metal-to-metal contact and rubbing during the sliding wear. At 400 °C and 760 °C, the fall in COF value could be from the formation of the oxides layer serving a solid lubricant on the Inconel 718 surface. The running-in time starts from 1.75 seconds which is exactly the same as for interaction of Inconel 718 with $Ti_{60}Al_{40}N$ coated disc.

For stainless steel 316L, continuous rise in friction with increase in temperature has been revealed in Figure 29 (b). An upward trend of COF value at all the three temperatures is in line with the COF characteristics of SS 316L interaction with $Ti_{60}Al_{40}N$, nonetheless, a negligible instability (fluctuation in COF amplitude) in friction values is distinguishable feature to what has been noticed in section 4.1 for SS 316L. The downward slope of COF at 760 °C goes even below the COF at 400 °C which predicts the formation of multiple oxides that were absent during SS 316L interaction with $Ti_{60}Al_{40}N$ at 760 °C. Moreover, a lower running-in time has been spotted here spanning to 2.25 seconds compared to section 4.1 findings.

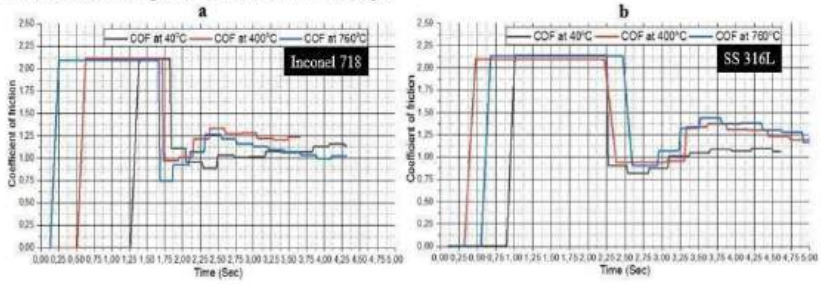

Figure 29: The evolution of COF at 40 °C, 400°C, and 760°C for (a) Inconel 718 (b) Stainless steel 316L, in a sliding wear test against $Ti_{40}Al_{60}N$ coated disc

Figure 30 convey the change in steady state average coefficient of friction with error bars showing standard deviation as a function of temperature. A different trend is seen here with higher friction values at 40 °C for Inconel 718. At 400 °C both materials show the same average steady state friction value higher than at 40 °C. Furthermore, at elevated temperatures, the COF decreases for

Inconel 718 whilst SS 316L repeats the same trend mentioned in section 4.1 about steady sate COF for SS 316L against $Ti_{60}Al_{40}N$.

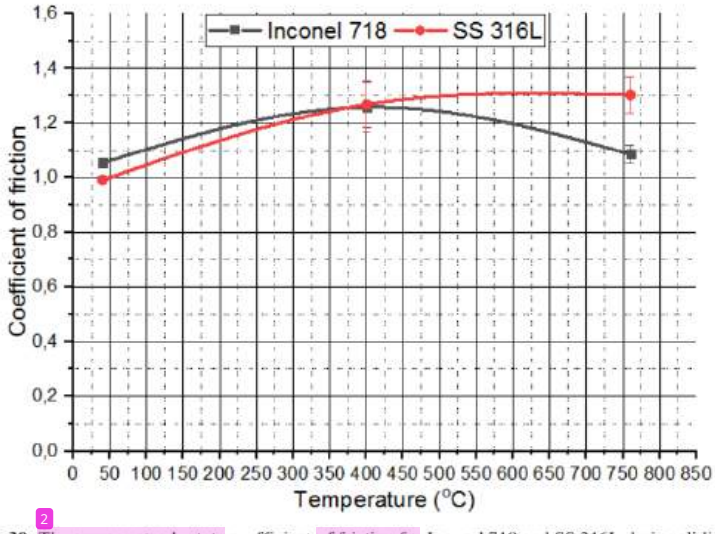

Figure 30: The average steady state coefficient of friction for Inconel 718 and SS 316L during sliding wear against $Ti_{40}Al_{60}N$

4.6. Effect of temperature on wear

The volume loss for pin and gain for disc surface with standard deviation as error bars for both Inconel 718 and SS 316L is given in Figure 31. The volume loss for Inconel 718 follows an inverse trend compared to Figure 21. Here, a consistent increment in material loss has been indicated by Inconel 718 at higher temperatures. The thermal conductivity of Inconel 718 is lower as compared to SS 316L, therefore, the transfer of available heat to the surface is not as pronounced leading to temperature rise at the contact zone. Consequently, the higher plastic deformation removes more material from Inconel 718 pin [81, 82].

For stainless steel 316L, apparently a negligible transfer of the material on the disc surface occur at 40 °C. The volumetric loss for pin is also very small suggesting the mere interaction of the pin asperities and surface irregularities. With rise in operating temperature, the volume loss increases along with an increment in transferred material. The highest volume loss and built-up material was observed at the same temperature of 760 °C contradicting to the SS 316L volume loss during interaction with $Ti_{60}Al_{40}N$ at elevated temperature. By comparing the SS 316L transferred material with Inconel 718 at 760 °C, a radical and pronounced difference has been found relating to the fact of lower strength of stainless steel 316L at higher temperature as compared to Inconel 718 [14] .

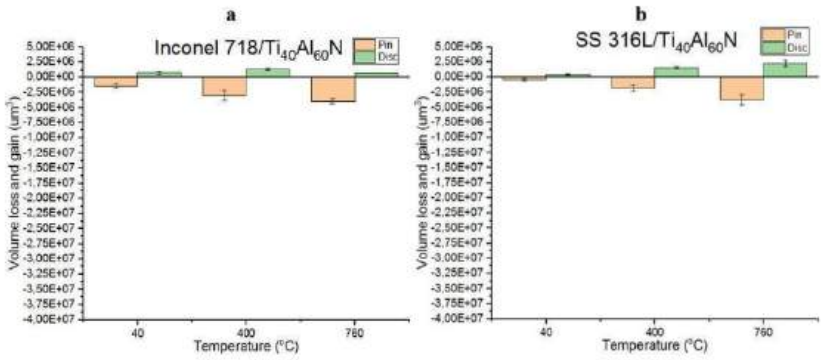

Figure 31: Volumetric loss and gain for Inconel 718 and SS 316L against $Ti_{40}Al_{60}N$

4.7. Worn surface analysis of Inconel 718 against $Ti_{40}Al_{60}N$ coating

The worn surfaces of the tested pin and disc are characterized with surface topographical measurements complemented via SEM/EDS analysis. At 40 °C, a very small amount of the material has transferred on to the coated disc mainly along the surface irregularities on the disc. An island of transferred material resulting from the reciprocating shearing action of the pin specimen over coating is observed. Nevertheless, parallel grooves are apparent on the pin surface resulting from interaction with work hardened transferred material. Therefore, mechanical transfer is the dominant wear mechanism at lower temperature. The pure mechanical interaction give rise to increase in friction value.

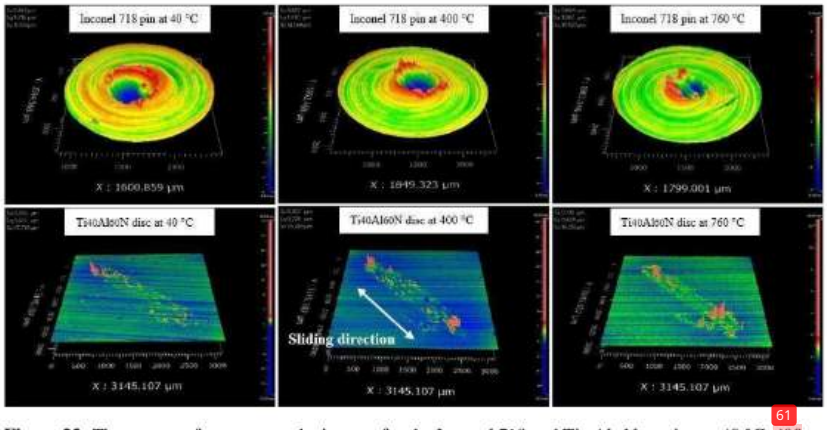

Figure 32: The worn surface topography images for the Inconel 718 and $Ti_{40}Al_{60}N$ coating at 40 °C, 400 °C and 760 °C

As the temperature is increased, the surface of the pin has undergone plastic deformation and displaced material to edges of the pin specimen. Surface topographical and SEM analysis elaborate the formation of parallel grooves and shallow scratches. The center of the pin shows smooth load bearing area with oxidized surface leading to decrease in friction value. The transferred material is more or less uniformly distributed in the center of the deposited layer with patches of work hardened adhered material on edges.

At 760 °C, the pin material faced excessive plastic deformation with large grooves on the surface. It looks like the higher temperature has thermally softened the pin surface which under compressive load and tangential forces experienced the displacement of large material chunks. Additionally, the center of the pin displays itself to be very smooth and acts as contacting area during the wear test under oxidized state triggering the reduction in friction value as shown in Figure 29 (a). The transferred material on the pin comprises of smooth surface with large patches of adhered material near both edges. The dominant wear seems to be a combination of adhesion, plastic deformation and oxidative wear [83, 91].

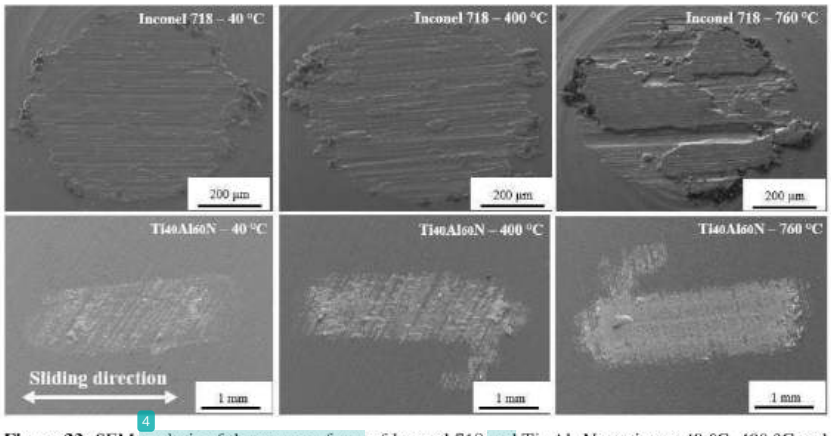

Figure 33: SEM analysis of the worn surfaces of Inconel 718 and $Ti_{40}Al_{60}N$ coating at 40 °C, 400 °C and 760 °C

To better understand the response of the coating, a detailed analysis at each temperature has been performed. Figure 34 exhibits the surfaces of the Inconel 718 pin and $Ti_{40}Al_{60}N$ coated disc. The transfer of the coating constituents on the pin surface confirms the degradation of the coating. A detailed SEM investigation demonstrated no peel off on the coating surface. Coating fragments are only found on the work hardened material present on the edge of the pin. Formation of the wear particles, ridges, and parallel grooves indicates the ploughing effect on pin surface. The absence of cracks on the surface of coating shown in Figure 34(c) dictates the high stability of coating at room temperature. The EDS spectra confirm the coating fragments as well as oxidization of the surface.

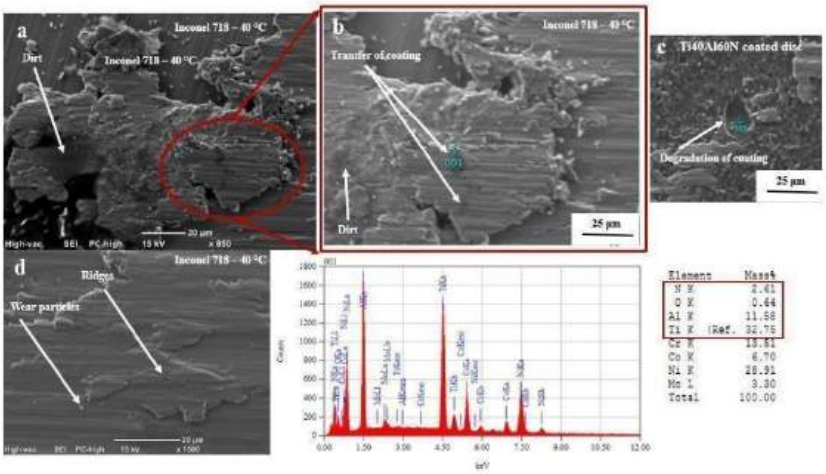

Figure 34: Transfer of coating on Inconel 718 and coating degradation at 40 °C

At 400 °C, multiple spots of the coating constituents have been found on the pin surface shown in Figure 35 (b) and (c). This infers a harsh mechanical interaction between the two surfaces.

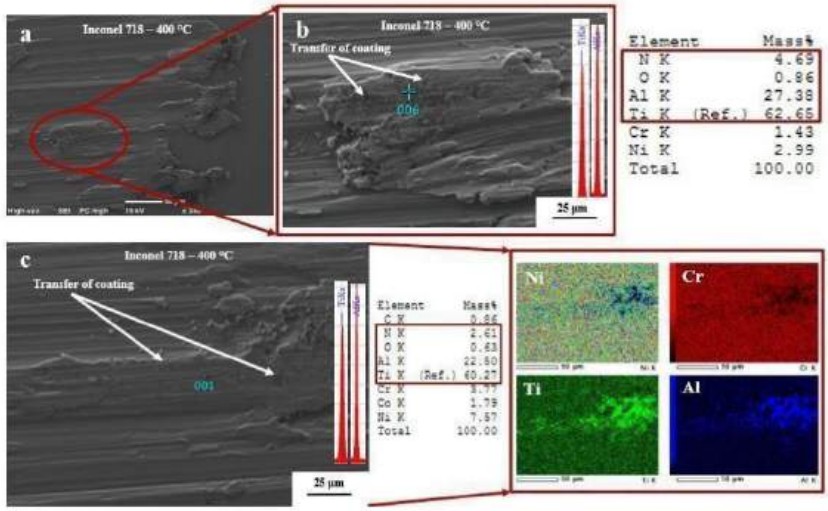

Figure 35: Transfer of $Ti_{40}Al_{60}N$ coating on Inconel 718 pin at 400 °C

The constituents of the coating are dispersed at various location on the pin surface. There is no sign of the coating transfer on the edges and are mostly found in the load bearing central area of the pin. EDS analysis in Figure 35 (b) and EDS mapping of Figure 35 (c) validates the observed findings at 400 °C.

Figure 36 highlights the phenomena happening on the surface of the disc at 400 °C. A severe damage to the coating resulted in rupture of the coating revealing the WC/Co substrate of the $Ti_{40}Al_{60}N$ disc. This damage in the form of peeling can originate from the local high shear stresses induced by the uneven surface created during the material transfer process. The sliding action of Inconel 718 on the harder WC/Co substrate coated with $Ti_{40}Al_{60}N$ coating generates cracks on the coating which are quite long and propagate through the coating surface. These fractured segments of the coating can come into the contact zone. The shearing action under fractured coating parts can increase the COF value. This might be the reason for the increase in COF of Inconel 718 at 400 °C.

Additionally, an increase in Aluminum (Al) content can render the coating structure to be less dense and grain size increases. This reduces the hardness, and consequently reduced mechanical and wear characteristics of the TiAlN coatings [93]. The increase in grain size correlates to the formation of the macro-particles that eventually increases the surface roughness [94].

Chipping phenomenon of the coating during wear also prevails at 400 °C. This is in accordance with the previous studies [67, 95, 96] conducted by different researcher proposing the idea that macro particles presence in coating promotes the chipping and fracture of coating. The fragments of chipping and from fracture of coating can serve as hard particles in the contact region which can promote the abrasive wear. Therefore, it can be discerned that adhesion along with the abrasion are the dominant wear mechanisms.

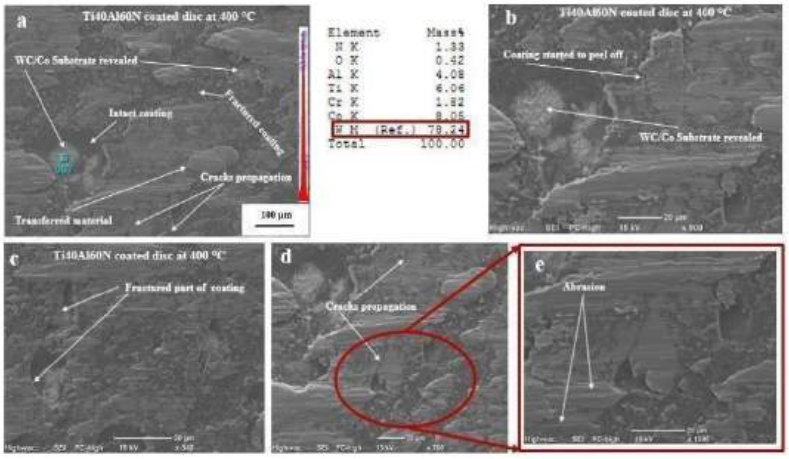

Figure 36: Degradation & fracture of $Ti_{40}Al_{60}N$ coating in a sliding wear test with Inconel 718 at 400 °C

At elevated temperature of 760 °C, the same observations have been made. Transfer of coating on the Inconel 718 is present in quite big marks in the center on the load bearing contact area. Figure 37 (b) and (c) manifests the coating transferred areas along with their EDS validation through EDS spectrum and mapping. EDS map shows very high concentration of transferred coating in the oxidized area.

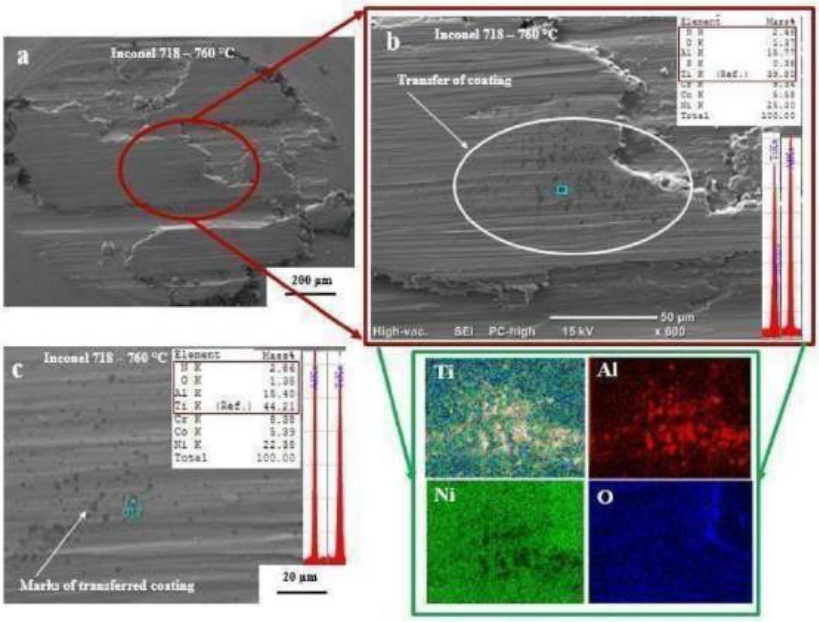

Figure 37: Transfer of $Ti_{40}Al_{60}N$ coating on Inconel 718 pin at 760 °C

Figure 38 presents the characterization of the coated disc through SEM/EDS analysis. The surface of the adhered material has undergone very severe oxidation with layers of porous oxide dispersed all over the adhered material. The surface of the coating has also been oxidized significantly. Transferred material has been hardened from the reciprocating action. Chipping of the transferred material under sliding movement is quite obvious with fractured segments dropped down from the main layer. Coating damage reveals the WC/Co substrate verified by the EDS analysis. The presence of high concentration of chromium in the adhered material along with aluminium proposes the formation of chromium oxides and aluminium oxides. Chromium oxides are usually very fine in pores and have high density. The finer nature of the chromium oxides can stop the further diffusion of oxygen resulting in a very fine protective layer on the surface of the adhered material [74, 91].

Moreover, the formation of the nano-porous aluminum oxides can also act as the protective and wear resistant layer thereby eliminating the direct metal-to-metal contact. As a result, reduced frictional behavior has been noted for Inconel 718 during interaction with $Ti_{40}Al_{60}N$ coating at 760 °C.

A detailed analysis of Figure 38 (d) refers to the large growing cracks in coating in a direction perpendicular to sliding direction. Cracks on the surface of adhered material were observed at different locations which might have developed due to the compressive and tangential stresses induced by the reciprocating sliding movement of the Inconel 718. A hardness analysis of the coating at elevated temperature can provide better insights into this response of coating [97, 98].

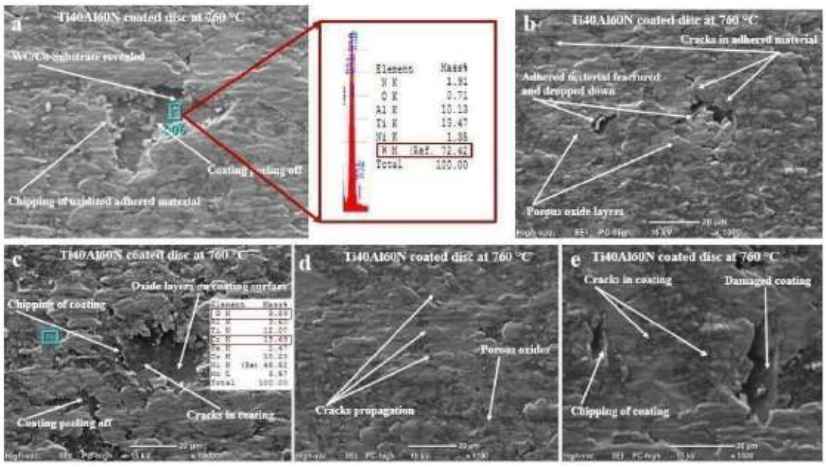

Figure 38: Degradation & fracture of $Ti_{40}Al_{60}N$ coating in a sliding wear test with Inconel 718 at 760 °C

4.8. Worn surface analysis of SS 316L against $Ti_{40}Al_{60}N$ coating

The worn surface of SS 316L characterized to gain insights about the active wear mechanism initiating the wear at three different temperatures through surface topography and SEM/EDS given in Figure 39 and 40. It can be noticed from the surface roughness values for both the pin and disc that transfer of material enhanced with increment in temperature significantly. There is more localized accumulation of plastically deformed material at 40 °C with less material on the edges. However, very small material has transferred along the surface irregularities at room temperature on disc surface. Hence, material transfer from disc surface seems more like mechanical deformation with some wide areas of deformed material. This behavior of SS 316L is completely different to what was seen during its interaction with $Ti_{60}Al_{40}N$ coating in section 4.3.

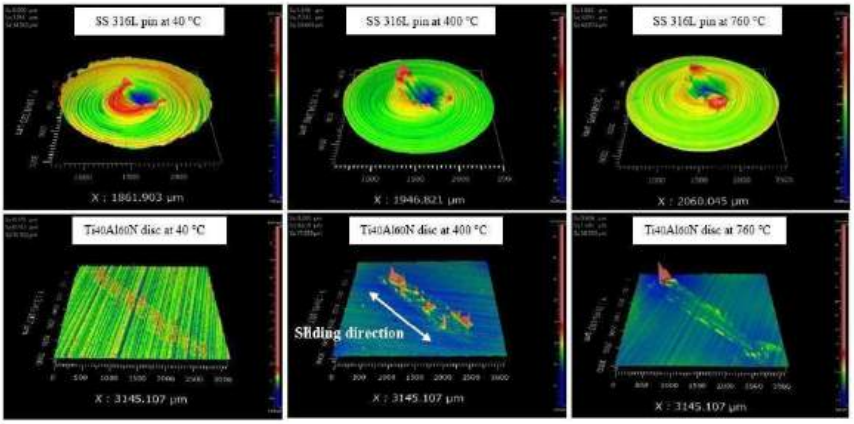

Figure 39: The worn surface topography images for the SS 316L and $Ti_{40}Al_{60}N$ coating at 40 °C, 400 °C and 760 °C

In addition to this, severe plastic deformation occurs at 400 °C governed by the low bulk strength of SS 316L at 400 °C. Large islands of deformed material are found on the edges of pin due to the displacement of plastically deformed material under compressive load. The grooves are wider and prominently located in central load bearing region as demonstrated in surface topographical analysis. Adhesion is the primary cause of the material transfer with transferred material height of 11 µm.

At elevated temperature of 760 °C, the surface of the coated disc looks very different from what was noticed for the previous two temperatures. The whole surface has oxidized with removal of the big patches of the material. A 34 µm height of transferred material complemented with deep and wide grooves indicates serious damage to pin surface probably as a result of low strength of SS 316L at higher temperature compared to Inconel 718.

A distinguishable characteristic noted here is the formation of a localized load bearing smooth surface on the edges which under severe oxidation can act as a solid lubricating surface. As a result, the frictional forces can significantly reduce due to preventing direct metal-to-metal contact. This phenomenon can be described as the reason of drop in COF for SS 316L at 760 °C in contrast to what we perceived during interaction with $Ti_{60}Al_{40}N$ coating [89, 93].

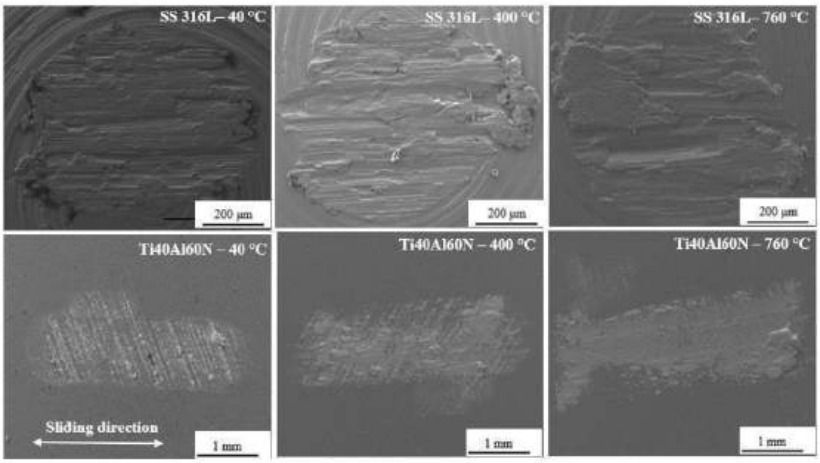

Figure 40: SEM analysis of worn surfaces of SS 316L and $Ti_{40}Al_{60}N$ coating at 40 °C, 400 °C and 760 °C

A SEM/EDS analysis of the worn surfaces of the coated disc and pin performed to scrutinize the active wear mechanism and degradation of coating. Figure 41 displays the coating transfer on the pin surface at 400 °C during the sliding wear of SS 316L against $Ti_{40}Al_{60}N$.

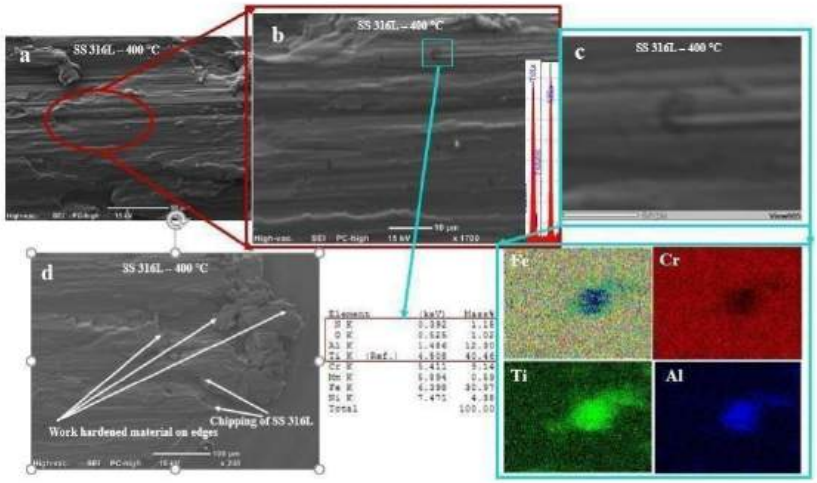

Figure 41: Transfer of $Ti_{40}Al_{60}N$ coating on SS 316L pin at 400 °C

Figure 41 (b) proposes that only a few spots of the transferred coating has been found on the pin surface. However, these coating fragments are not uniform and only a very few regions over the surface shows enough intensity to notice coating transfer. The surface of the pin has hardened plastically deformed material on the edges which is oxidized. In addition to this, chipping of SS 316L on the load bearing area indicates the removal of hard material on pin surface under reciprocating compressive load.

The surface of the coated disc indicates the degradation and rupture of the coating in Figure 42. Tungsten carbide is clearly visible with oxidized surface in Figure 42(d). Chipping and fracture of the transferred as well as the coating is quite noticeable for the adhered material and coating. The chipping of the transferred built-up material has occurred which can be referred to the smooth surface in the form of grooves on the adhered material. During the sliding test, the adhered material can readily oxidize and fracture under the applied compressive shearing load. Moreover, the sticking of adhered material to the coating surface and their subsequent removal due to fracture during the wear process can results in spallation or peeling off of the coating underneath. This phenomenon of the transferred material adherence followed by their removal can increase the friction force and eventually coefficient of friction. This might be the reason behind the gradual increase of COF of SS 316L during sliding wear against $Ti_{40}Al_{60}N$ at 400 °C [74, 100].

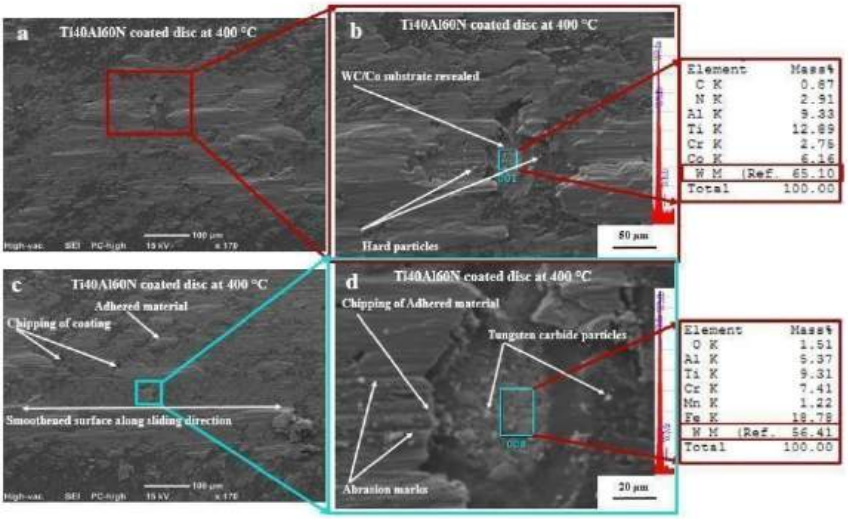

Figure 42: Degradation & chipping of $Ti_{40}Al_{60}N$ coating in a sliding wear test with SS 316L at 400 °C

Furthermore, the sliding action under compressive load can remove some hard tungsten carbide particles from the substrate surface which during shearing action promote the abrasive wear on the surface of adhered material. The presence of the abrasive marks on the surface of adhered material

has been shown in a magnified SEM micrograph in Figure 42(d). As a result, the adhesion and three body abrasive wear are the main wear mechanisms at 400 °C.

At elevated temperature of 760 °C, the surface of the SS 316L has oxidized with patches of the oxides all over the surface. The micrographs in Figure 43 depicts the wear mechanism happening at higher temperature. A closer look at Figure 43 (a) and (b) shows the high volume of the abrasive marks and the ploughing of the surface on the SS 316L pin. A very detailed SEM/EDS analysis has been performed on the disc to discover the reason behind ploughing. The hard particles of the tungsten carbide detected by the EDS in the area manifested in Figure 43(c). Areas of high concentration of tungsten carbide particles has been found on the edges of the pin. These particles are present in bigger size as compared to what was observed at 400 °C. Thus, hard particles protrude through the soft pin material surface during sliding action leading to ploughing wear mechanism on the disc.

In addition to this, carbide particles in smaller size are dispersed over the whole pin surface acting as the wear particles accelerating the three-body abrasive wear. This generates multiple abrasion marks and scratches all over the pin surface exhibited in Figure 43 (a) and (b).

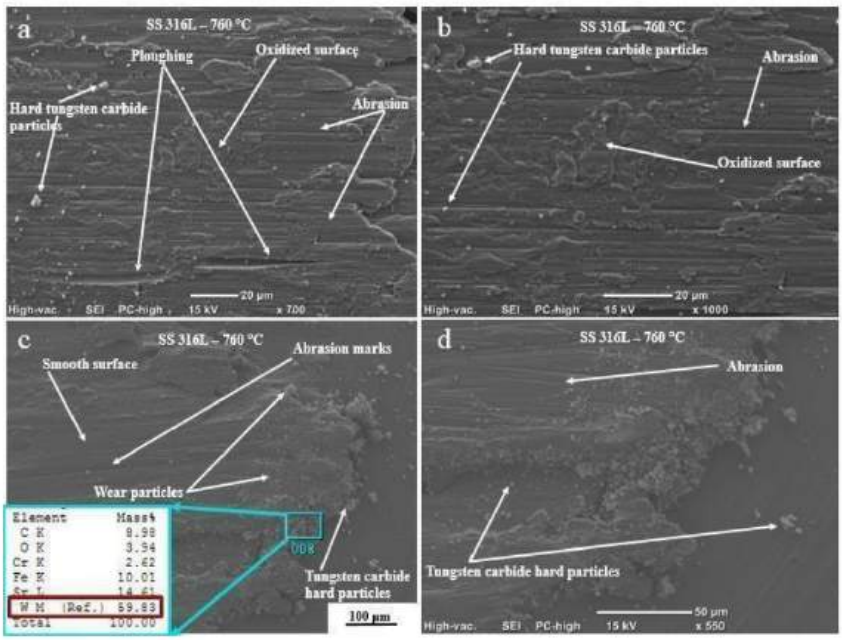

Figure 43: Wear of SS 316L pin during sliding wear against $Ti_{40}Al_{60}N$ coating at 760 °C

The worn surface analysis of the coated disc with adhered material at 760 °C is shown in Figure 44. It can be seen from Figure 44(a) that built-up material resulting from the material transfer has undergone chipping and fracture disconnecting it from the thin companion layer. The surface of the coated disc has been oxidized with smooth thin layers of the transferred material in the center of the transferred material given in Figure 44(b). These layers are oxidized and due to the high temperature in the center (as velocity of reciprocating sliding pin is maximum in center and instantaneously zero at the edges) and high pressure from compressive load, can promote further chemical reaction between the $Ti_{40}Al_{60}N$ coating and stainless steel pin surface [74, 101].

Figure 44(c) presents the very oxidized surface of the patches of the adhered material. The cracks and fracture of the oxidized adhered material were observed at elevated temperature on different places. The uniform porous structure of the oxides has been revealed in Figure 44(e). The pores are dense with small size uniformly distributed on the adhered material surface. EDS analysis results shows the presence of aluminium, titanium and chromium on the surface of porous oxide layer. This oxide layer seems to have multiple complex oxides which can be further analyzed at the nanoscale.

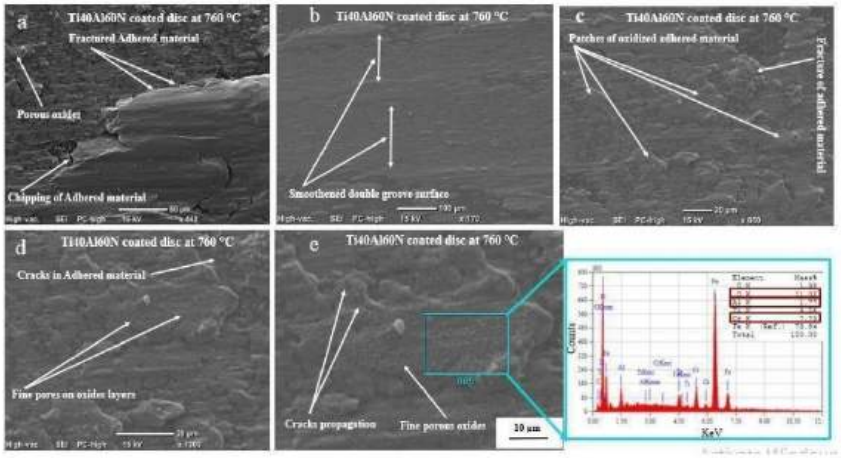

Figure 44: Stability analysis of $Ti_{40}Al_{60}N$ coating in a sliding wear test with SS 316L at 760 °C

In order to achieve the 760 °C temperature on the disc surface, the preheating of the disc prior to running the test can lead to formation of layer structure of oxides with different sublayers altering the contact mechanism occurring during the wear. In the previous literature, formation of double layer oxides with lower sublayer of titanium oxides and upper sublayer of aluminium oxide has been reported during the heating of TiAlN coated (WC/Co substrate) disc [91, 102–104].

Besides this, the porous oxides layers on the surface of the transferred material and oxidized pin surface can chemically react with each other during the sliding wear. The contact between the oxides can eliminate the direct contact of both surfaces reducing the friction giving rise to new tribological properties. This type of formation of oxides structure could be the plausible cause of a slight fall in friction coefficient for SS 316L sliding against $Ti_{40}Al_{60}N$ coating at 760 °C. This behavior of drop in coefficient of friction contrast with what was observed for sliding wear of SS 316L with $Ti_{60}Al_{40}N$ discussed in section 4.1. Eventually, the presence of hard particles on the pin surface shown in Figure 43(c) and (d) can abrade the oxides layers and removing the oxide-to-oxide contact. Therefore, adhesion, abrasion and oxidation are the wear mechanism for SS 316L during a sliding wear test with $Ti_{40}Al_{60}N$ coating at 760 °C.

Chapter 5

5. Conclusions

In this thesis, an experimental investigation has been carried out to understand the wear initiation mechanism at different temperatures during the tribological interaction of difficult to machine super alloys and TiAlN coatings. Furthermore, tribological performance of Inconel 718 and low carbon stainless steel 316 (SS 316L) at elevated temperature has been elucidated.

The main conclusions from this research work are as follows:

- The variation in temperature influences the frictional response and wear of both materials and coating compositions ($Ti_{60}Al_{40}N$ and $Ti_{40}Al_{60}N$). Generally, Inconel 718 showed increase in friction up to 400 °C followed by a drop down in value at 760 °C. Stainless steel 316L (SS 316L) shown a continuous increase in friction with temperature value for both coatings composition.
- Average steady state coefficient of friction at 40 °C for Inconel 718 and SS 316 with $Ti_{60}Al_{40}N$ has almost the same value with the former one experiencing fall in friction value with later one soaring up in friction coefficient at 760 °C. Nonetheless, for $Ti_{40}Al_{60}N$, Inconel 718 friction response is higher than SS 316L at 40 °C and interestingly sharing the same value at 400 °C with subsequent fall and rise in friction value for Inconel 718 and SS 316L respectively.
- Wear volume of Inconel 718 is very high at room temperature with $Ti_{60}Al_{40}N$ coating and demonstrate a gradual decrease with rise in temperature. However, opposite to this was observed against $Ti_{40}Al_{60}N$ with highest wear at 760 °C. Stainless steel 316L shows highest volume loss at 400 °C and lowest at room temperature against $Ti_{60}Al_{40}N$ coating. During sliding against $Ti_{40}Al_{60}N$ coating, a trend similar to Inconel 718 noticed i.e. augmented wear volume with rise in temperatures with a maximum value at 760 °C.
- The wear initiation mechanism is purely mechanical interaction of Inconel 718 and stainless steel 316L with surface irregularities of both coating at 40 °C. With $Ti_{60}Al_{40}N$ coating at 400 °C, Inconel 718 showed adhesive wear and abrasion marks on the surface. Nevertheless, at 760 °C, adhesion and oxidation are the primary wear mechanism. No damage to the coating surface noticed.
- Stainless steel 316L underwent severe plastic deformation at 400 °C against $Ti_{60}Al_{40}N$ due to thermal softening and low bulk strength at 400 °C. Purely adhesion phenomena dominating the wear was conceived at 760 °C. The surface of the coating has not been damaged at higher temperatures even.
- For $Ti_{40}Al_{60}N$ coating, Inconel 718 surface showed transfer of coating constituents at room temperature with some degraded regions of coating along the transferred material. At 400 °C, coating was locally destroyed and high amount of coating fragments appeared on SS 316L pin surface. Chipping, abrasive wear and adhesive wear are main wear mechanisms. At elevated temperature of 760 °C, formation of less dense porous oxides was spotted generating cracks, chipping and abrasive wear on the coating and adhered material surface.

The coating showed fracture and peeled off at 760 °C. Adhesion, abrasion, oxidation and chipping are the primary wear mechanism.

- $Ti_{40}Al_{60}N$ coating proved to be very stable for stainless steel 316L at room temperature with no transfer of coating on SS 316L pin surface. However, SS 316L has plastically deformed at 40 °C. At 400 °C, the coating was ruptured revealing the tungsten carbide substrate at different locations and got transferred on the SS 316L pin surface in the form of circular spots. Sings of abrasion, chipping, and adhesion are the main wear mechanisms. At high temperature conditions of 760 °C, SS 316L experienced the formation of porous oxides, three body abrasive wear and ploughing as dominant wear mechanisms. Besides this, the adhered material on coating surface oxidized with cracking, chipping, oxidative wear along with adhesive wear as prevailing wear mechanisms.

From the above conclusions, it can be stated that $Ti_{60}Al_{40}N$ coating, the tribological performance and wear is mainly governed by the transfer of the material and subsequent formation of built-up material for Inconel 718 and SS 316L. On the other hand, for $Ti_{40}Al_{60}N$ coating, the rupture of coating and oxidation of adhered material surface controls the subsequent wear mechanism for both super alloys.

5.2. Future work

This research work can further be investigated in followings ways:

- The micro-structure of the coatings should be analyzed before performing wear test to examine the temperature effect on structure changes in the coatings and their tribological behavior.
- Further analysis of the Inconel 718 and SS 316L pins can be performed by etching to reveal the microstructural variations at higher temperature.
- Correlating the high temperature hardness of coatings with their tribological performance.

References

[1] L. Supriyanti, "World of Steel: Economic & Social Impact of the Steel Industry," *Insights*, Feb. 2022. [Online]. Available: https://liwasupriyanti.com/world-of-steel-economic-social-impact-of-the-steel-industry/

[2] P. V. Moghaddam, *On the role of microstructure in wear of nanostructured bainitic steels*, PhD disser. Luleå University of Technology, Luleå, 2020. [Online]. Available: http://www.diva-portal.org/smash/get/diva2:1433487/FULLTEXT01.pdf

[3] F. Pervaiz, S. M. Asce, M. A. Hummel, and A. M. Asce, "Effects of Climate Change and Urbanization on Bridge Flood Vulnerability : A Regional Assessment for Harris County , Texas," vol. 24, no. 3, pp. 1–10, 2023, doi: 10.1061/NHREFO.NHENG-1720.

[4] C. T. Sims, "A History of Superalloy Metallurgy for Superalloy Metallurgists," in *Superalloys 1984 (Fifth International Symposium)*, TMS, 1984, pp. 399–419. doi: 10.7449/1984/Superalloys_1984_399_419.

[5] M. Asif *et al.*, "The Effect of Infrared Laser Irradiation on the Surface Morphology and Electrical Properties of Zinc Metal," *Physchem*, vol. 3, no. 1, pp. 22–33, 2022, doi: 10.3390/physchem3010003.

[6] M. J. Donachie, *Superalloys: A Technical Guide (06128G) - Hardcover*, Second. ASM International, 2002. [Online]. Available: https://www.abebooks.com/9780871707499/Superalloys-Technical-Guide-06128G-Matthew-0871707497/plp

[7] L. Makaji, M. Gaikhe, V. Mahabale, and N. Gharat, "A Review on Tool Wear Mechanisms in Milling of Super Alloy," *Int. J. Sci. Eng. Res.*, vol. 6, no. 12, pp. 220–227, 2015.

[8] D. Ulutan and T. Ozel, "Machining induced surface integrity in titanium and nickel alloys: A review," *Int. J. Mach. Tools Manuf.*, vol. 51, no. 3, pp. 250–280, Mar. 2011, doi: 10.1016/J.IJMACHTOOLS.2010.11.003.

[9] "What is a Superalloy: Types, Manufacturing & Applications," *Metal Supermarket*, 2023. https://www.metalsupermarkets.com/superalloys-types-manufacturing-applications/ (accessed May 04, 2023).

[10] G. R. Thellaputta, P. S. Chandra, and C. S. P. Rao, "Machinability of Nickel Based Superalloys: A Review," *Mater. Today Proc.*, vol. 4, no. 2, pp. 3712–3721, 2017, doi: 10.1016/j.matpr.2017.02.266.

[11] A. Tayal, N. S. Kalsi, and M. K. Gupta, "Machining of superalloys: A review on machining parameters, cutting tools, and cooling methods," *Mater. Today Proc.*, vol. 43, pp. 1839–1849, Jan. 2021, doi: 10.1016/J.MATPR.2020.10.815.

[12] K. Xu, B. Zou, C. Huang, Y. Yao, H. Zhou, and Z. Liu, "Machinability of Hastelloy C-276 using hot-pressed sintered Ti(C7N3)-based cermet cutting tools," *Chinese J. Mech. Eng. (English Ed.*, vol. 28, no. 3, pp. 599–606, 2015, doi: 10.3901/CJME.2015.0316.031.

[13] W. Grzesik, "Trends in Metal Cutting Theory and Practice," *Adv. Mach. Process. Met. Mater.*, pp. 21–34, Jan. 2017, doi: 10.1016/B978-0-444-63711-6.00003-X.

[14] S. Saketi, U. Bexell, J. Östby, and M. Olsson, "On the diffusion wear of cemented carbides in the turning of AISI 316L stainless steel," *Wear*, vol. 430–431, pp. 202–213, Jul. 2019, doi: 10.1016/J.WEAR.2019.05.010.

[15] S. Ranganathan, T. Senthilvelan, and G. Sriram, "Evaluation of machining parameters of hot turning of stainless steel (type 316) by applying ANN and RSM," *Mater. Manuf. Process.*, vol. 25, no. 10, pp. 1131–1141, 2010, doi: 10.1080/10426914.2010.489790.

[16] J. Nomani, A. Pramanik, T. Hilditch, and G. Littlefair, "Machinability study of first generation duplex (2205), second generation duplex (2507) and austenite stainless steel during drilling process," *Wear*, vol. 304, no. 1–2, pp. 20–28, Jul. 2013, doi: 10.1016/J.WEAR.2013.04.008.

[17] S. S. Gill, H. Singh, R. Singh, and J. Singh, "Flank wear and machining performance of cryogenically treated tungsten carbide inserts," *Mater. Manuf. Process.*, vol. 26, no. 11, pp. 1430–1441, 2011, doi: 10.1080/10426914.2011.557128.

[18] L. Jiang, H. Hänninen, J. Paro, and V. Kauppinen, "Active wear and failure mechanisms of TiN-coated high speed steel and TiN-coated cemented carbide tools when machining powder metallurgically made stainless steels," *Metall. Mater. Trans. A Phys. Metall. Mater. Sci.*, vol. 27, no. 9, pp. 2796–2808, 1996, doi: 10.1007/BF02652372.

[19] A. Atarsia, "Machining Heat-Resistant Super Alloy(HRSA) with YG-1 – Machining Solutions," *Cutting Tools Newsletter*, Jun. 2022. [Online]. Available: https://www.yg1.kr/storage/newsletter/VOL25all/Mainnews.html

[20] J. L. Endrino, G. S. Fox-Rabinovich, and C. Gey, "Hard AlTiN, AlCrN PVD coatings for machining of austenitic stainless steel," *Surf. Coatings Technol.*, vol. 200, no. 24, pp. 6840–6845, Aug. 2006, doi: 10.1016/j.surfcoat.2005.10.030.

[21] I. Korkut, M. Kasap, I. Ciftci, and U. Seker, "Determination of optimum cutting parameters during machining of AISI 304 austenitic stainless steel," *Mater. Des.*, vol. 25, no. 4, pp. 303–305, Jun. 2004, doi: 10.1016/J.MATDES.2003.10.011.

[22] T. Akasawa, H. Sakurai, M. Nakamura, T. Tanaka, and K. Takano, "Effects of free-cutting additives on the machinability of austenitic stainless steels," *J. Mater. Process. Technol.*, vol. 143–144, no. 1, pp. 66–71, Dec. 2003, doi: 10.1016/S0924-0136(03)00321-2.

[23] W. S. Lin, "The study of high speed fine turning of austenitic stainless steel," *J. Achiev. Mater. Manuf.*, vol. 27, no. 2, pp. 191–194, 2008.

[24] J. Rodriguez, P., Fernandez, A.I., Labarga, J.E. and Garcia, "Estimation of optimal cutting conditions for austenitic stainless steels machining," in *Proceedings of ECTC*, Miami, Florida, USA., 2008.

[25] M. A. Khan, A. S. Kumar, S. T. Kumaran, M. Uthayakumar, and T. J. Ko, "Effect of Tool Wear on Machining GFRP and AISI D2 Steel Using Alumina Based Ceramic Cutting Tools," *Silicon*, vol. 11, no. 1, pp. 153–158, 2019, doi: 10.1007/s12633-018-9839-7.

[26] P. M. Mashinini, H. Soni, and K. Gupta, "Investigation on dry machining of stainless steel 316 using textured tungsten carbide tools," *Mater. Res. Express*, vol. 7, no. 1, 2020, doi: 10.1088/2053-1591/ab5630.

[27] D. Dudzinski, A. Devillez, A. Moufki, D. Larrouquère, V. Zerrouki, and J. Vigneau, "A review of developments towards dry and high speed machining of Inconel 718 alloy," *Int. J. Mach. Tools Manuf.*, vol. 44, no. 4, pp. 439–456, Mar. 2004, doi: 10.1016/S0890-6955(03)00159-7.

[28] A. Devillez, F. Schneider, S. Dominiak, D. Dudzinski, and D. Larrouquere, "Cutting forces and wear in dry machining of Inconel 718 with coated carbide tools," *Wear*, vol. 262, no. 7–8, pp. 931–942, Mar. 2007, doi: 10.1016/J.WEAR.2006.10.009.

[29] M. R., Arunachalam, M.A., "Machining Science and Technology : An International MACHINABILITY OF NICKEL-BASED HIGH TEMPERATURE ALLOYS," *Mach. Sci. Technol. An Int. J.*, vol. 4:1, no. September, pp. 37–41, 2014.

[30] S. Olovsjö, A. Wretland, and G. Sjöberg, "The effect of grain size and hardness of wrought Alloy 718 on the wear of cemented carbide tools," *Wear*, vol. 268, no. 9–10, pp. 1045–1052, Mar. 2010, doi: 10.1016/J.WEAR.2010.01.017.

[31] H. Hayama, H. Kiyota, F. Itoigawa, and T. Nakamura, "Size effect in machining on initial tool wear in heat-resistant alloy cutting," *Key Eng. Mater.*, vol. 656–657, pp. 357–362, 2015, doi: 10.4028/www.scientific.net/KEM.656-657.357.

[32] M. A. Xavior, M. Manohar, P. Jeyapandiarajan, and P. M. Madhukar, "Tool Wear Assessment During Machining of Inconel 718," *Procedia Eng.*, vol. 174, pp. 1000–1008, Jan. 2017, doi: 10.1016/J.PROENG.2017.01.252.

[33] M. M. Noor, K. Kadirgama, H. H. Habeeb, M. M. Rahman, and B. Mohammad, "Performance of carbide cutting tools when machining of nickel based alloy," *Int. J. Mater. Form.*, vol. 3, no. SUPPL. 1, pp. 475–478, 2010, doi: 10.1007/s12289-010-0810-4.

[34] G. Akhyar Ibrahim, C. H. Che Haron, J. Abdul Ghani, A. Y. M. Said, and M. Z. Abu Yazid, "Performance of PVD-coated carbide tools when turning inconel 718 in dry machining," *Adv. Mech. Eng.*, vol. 2011, no. January, 2011, doi: 10.1155/2011/790975.

[35] A. R. Lansdown, "Molybdenum disulphide lubrication," in *Tribology Series 35*, Elsevier, 1999.

[36] J. Hardell, *Tribology of Hot Forming Tool and High Strength Steels*. 2009. [Online]. Available: https://www.diva-portal.org/smash/get/diva2:999138/FULLTEXT01.pdf

[37] H. Czichos, "Tribological Systems. In: Introduction to Systems Thinking and Interdisciplinary Engineering . Synthesis Lectures on Engineering, Science, and Technology.," Springer, Cham, 2022, pp. 37–71. doi: 10.1007/978-3-031-18239-6_3.

[38] A. C. Gonçalves, "Maintenance of Reducers with an Unbalanced Load Through Vibration and Oil Analysis Predictive Techniques," in *Recent Advances in Vibrations Analysis*, N. Baddour, Ed., 2021, p. 236.

[39] R. Wang, D. Yang, W. Wang, F. Wei, Y. Lu, and Y. Li, "Tool Wear in Nickel-Based

Superalloy Machining: An Overview," *Processes*, vol. 10, no. 11, 2022, doi: 10.3390/pr10112380.

[40] D. Zhu, X. Zhang, and H. Ding, "Tool wear characteristics in machining of nickel-based superalloys," *Int. J. Mach. Tools Manuf.*, vol. 64, pp. 60–77, Jan. 2013, doi: 10.1016/J.IJMACHTOOLS.2012.08.001.

[41] L. Li, N. He, M. Wang, and Z. G. Wang, "High speed cutting of Inconel 718 with coated carbide and ceramic inserts," *J. Mater. Process. Technol.*, vol. 129, no. 1–3, pp. 127–130, Oct. 2002, doi: 10.1016/S0924-0136(02)00590-3.

[42] Z. P. Hao, Y. H. Fan, J. Q. Lin, F. F. Ji, and X. Liu, "New observations on wear mechanism of self-reinforced SiAlON ceramic tool in milling of Inconel 718," *Arch. Civ. Mech. Eng.*, vol. 17, no. 3, pp. 467–474, May 2017, doi: 10.1016/J.ACME.2016.12.011.

[43] E. Liu, W. An, Z. Xu, and H. Zhang, "Experimental study of cutting-parameter and tool life reliability optimization in inconel 625 machining based on wear map approach," *J. Manuf. Process.*, vol. 53, pp. 34–42, May 2020, doi: 10.1016/J.JMAPRO.2020.02.006.

[44] C. Wang, W. Ming, and M. Chen, "Milling tool's flank wear prediction by temperature dependent wear mechanism determination when machining Inconel 182 overlays," *Tribol. Int.*, vol. 104, pp. 140–156, Dec. 2016, doi: 10.1016/J.TRIBOINT.2016.08.036.

[45] S. Chihaoui, M. A. Yallese, S. Belhadi, A. Belbah, K. Safi, and A. Haddad, "Coated CBN cutting tool performance in green turning of gray cast iron EN-GJL-250: modeling and optimization," *Int. J. Adv. Manuf. Technol.*, vol. 113, no. 11–12, pp. 3643–3665, 2021, doi: 10.1007/s00170-021-06820-1.

[46] B. Li, W. Ding, M. Li, and X. Zhang, "Tool wear behavior of alumina abrasive wheels during grinding FGH96 powder metallurgy nickel-based superalloy," *Procedia CIRP*, vol. 101, pp. 182–185, Jan. 2021, doi: 10.1016/J.PROCIR.2020.04.161.

[47] R. Zimmermann, D. Welling, T. Venek, P. Ganser, and T. Bergs, "Tool wear progression of SiAlON ceramic end mills in five-axis high-feed rough machining of an Inconel 718 BLISK," *Procedia CIRP*, vol. 101, pp. 13–16, Jan. 2021, doi: 10.1016/J.PROCIR.2021.02.003.

[48] N. Potthoff and P. Wiederkehr, "Fundamental investigations on wear evolution of machining Inconel 718," *Procedia CIRP*, vol. 99, pp. 171–176, Jan. 2021, doi: 10.1016/J.PROCIR.2021.03.024.

[49] E. O. Ezugwu, J. Bonney, and Y. Yamane, "An overview of the machinability of aeroengine alloys," *J. Mater. Process. Technol.*, vol. 134, no. 2, pp. 233–253, Mar. 2003, doi: 10.1016/S0924-0136(02)01042-7.

[50] Y. C. Chen and Y. S. Liao, "Study on wear mechanisms in drilling of Inconel 718 superalloy," *J. Mater. Process. Technol.*, vol. 140, no. 1–3, pp. 269–273, Sep. 2003, doi: 10.1016/S0924-0136(03)00792-1.

[51] O. A. Olufayo, H. Che, V. Songmene, C. Katsari, and S. Yue, "Machinability of Rene 65 superalloy," *Materials (Basel).*, vol. 12, no. 12, 2019, doi: 10.3390/ma12122034.

[52] D. Jianxin, L. Lili, L. Jianhua, Z. Jinlong, and Y. Xuefeng, "Failure mechanisms of TiB2 particle and SiC whisker reinforced Al2O3 ceramic cutting tools when machining nickel-based alloys," *Int. J. Mach. Tools Manuf.*, vol. 45, no. 12–13, pp. 1393–1401, Oct. 2005, doi: 10.1016/J.IJMACHTOOLS.2005.01.033.

[53] M. S. Kasim, C. H. Che Haron, J. A. Ghani, M. A. Sulaiman, and M. Z. A. Yazid, "Wear mechanism and notch wear location prediction model in ball nose end milling of Inconel 718," *Wear*, vol. 302, no. 1–2, pp. 1171–1179, Apr. 2013, doi: 10.1016/J.WEAR.2012.12.040.

[54] E. O. Ezugwu, "Key improvements in the machining of difficult-to-cut aerospace superalloys," *Int. J. Mach. Tools Manuf.*, vol. 45, no. 12–13, pp. 1353–1367, Oct. 2005, doi: 10.1016/J.IJMACHTOOLS.2005.02.003.

[55] X. Wu, J. Shen, F. Jiang, H. Wu, and L. Li, "Study on the oxidation of WC-Co cemented carbide under different conditions," *Int. J. Refract. Met. Hard Mater.*, vol. 94, p. 105381, Jan. 2021, doi: 10.1016/J.IJRMHM.2020.105381.

[56] R. S. Pawade, S. S. Joshi, P. K. Brahmankar, and M. Rahman, "An investigation of cutting forces and surface damage in high-speed turning of Inconel 718," *J. Mater. Process. Technol.*, vol. 192–193, pp. 139–146, Oct. 2007, doi: 10.1016/J.JMATPROTEC.2007.04.049.

[57] A. E. Diniz, R. Micaroni, and A. Hassui, "Evaluating the effect of coolant pressure and flow rate on tool wear and tool life in the steel turning operation," *Int. J. Adv. Manuf. Technol.*, vol. 50, no. 9–12, pp. 1125–1133, 2010, doi: 10.1007/s00170-010-2570-1.

[58] S. Do Nascimento Rosa, A. E. Diniz, D. Neves, B. B. Salles, and S. S. Guerreiro, "Analysis of the life of cemented carbide drills with modified surfaces," *Int. J. Adv. Manuf. Technol.*, vol. 71, no. 9–12, pp. 2125–2136, 2014, doi: 10.1007/s00170-013-5598-1.

[59] C. A. De Oliveira Junior, A. E. Diniz, and R. Bertazzoli, "Correlating tool wear, surface roughness and corrosion resistance in the turning process of super duplex stainless steel," *J. Brazilian Soc. Mech. Sci. Eng.*, vol. 36, no. 4, pp. 775–785, 2014, doi: 10.1007/s40430-013-0119-6.

[60] A. Braghini Junior, A. E. Diniz, and F. T. Filho, "Tool wear and tool life in end milling of 15-5 PH stainless steel under different cooling and lubrication conditions," *Int. J. Adv. Manuf. Technol.*, vol. 43, no. 7–8, pp. 756–764, 2009, doi: 10.1007/s00170-008-1744-6.

[61] J. Thompson, "Identifying tool wear," *Canadian Metalworking*, 2018. Accessed: May09, 2023. [Online]. Available: https://www.canadianmetalworking.com/canadianmetalworking/article/cuttingtools/identifying-tool-wear

[62] P. de Vos, "Tool Wear Patterns & How to optimize them," *SECO Tools*, 2023. [Online]. Available: https://www.secotools.com/article/122073?language=en

[63] P. A. Dearnley and E. M. Trent, "Wear mechanisms of coated carbide tools," *Met. Technol.*, vol. 9, no. 1, pp. 60–75, 1982, doi: 10.1179/030716982803285909.

[64] P. A. Dearnley, "Rake and flank wear mechanisms of coated cemented carbides," *Surf. Eng.*, vol. 1, no. 1, pp. 43–58, 1985, doi: 10.1179/sur.1985.1.1.43.

[65] A. Höling, L. Hultman, M. Odén, J. Sjölén, and L. Karlsson, "Mechanical properties and machining performance of Ti1-xAlxN-coated cutting tools," *Surf. Coatings Technol.*, vol. 191, no. 2–3, pp. 384–392, 2005, doi: 10.1016/j.surfcoat.2004.04.056.

[66] N. Sharma and K. Gupta, "Influence of coated and uncoated carbide tools on tool wear and surface quality during dry machining of stainless steel 304," *Mater. Res. Express*, vol. 6, no. 8, 2019, doi: 10.1088/2053-1591/ab1e59.

[67] S. Saketi, J. Östby, and M. Olsson, "Influence of tool surface topography on the material transfer tendency and tool wear in the turning of 316L stainless steel," *Wear*, vol. 368–369, pp. 239–252, Dec. 2016, doi: 10.1016/J.WEAR.2016.09.023.

[68] U. Wiklund *et al.*, "Experimental and theoretical studies on stainless steel transfer onto a TiN-coated cutting tool," *Acta Mater.*, vol. 59, no. 1, pp. 68–74, Jan. 2011, doi: 10.1016/J.ACTAMAT.2010.09.005.

[69] J. Gerth *et al.*, "Adhesion phenomena in the secondary shear zone in turning of austenitic stainless steel and carbon steel," *J. Mater. Process. Technol.*, vol. 214, no. 8, pp. 1467–1481, Aug. 2014, doi: 10.1016/J.JMATPROTEC.2014.01.017.

[70] W. Grzesik, Z. Zalisz, S. Krol, and P. Nieslony, "Investigations on friction and wear mechanisms of the PVD-TiAlN coated carbide in dry sliding against steels and cast iron," *Wear*, vol. 261, no. 11–12, pp. 1191–1200, Dec. 2006, doi: 10.1016/J.WEAR.2006.03.004.

[71] K. Zhang, J. Deng, X. Guo, L. Sun, and S. Lei, "Studyon the adhesion and tribological behavior of PVD TiAlN coatings with a multi-scale textured substrate surface," *Int. J. Refract. Met. Hard Mater.*, vol. 72, pp. 292–305, Apr. 2018, doi: 10.1016/J.IJRMHM.2018.01.003.

[72] J. Hardell and B. Prakash, "Tribological performance of surface engineered tool steel at elevated temperatures," *Int. J. Refract. Met. Hard Mater.*, vol. 28, no. 1, pp. 106–114, Jan. 2010, doi: 10.1016/J.IJRMHM.2009.07.009.

[73] C. Courbon, M. Fallqvist, J. Hardell, R. M'Saoubi, and B. Prakash, "Adhesion tendency of PVD TiAlN coatings at elevated temperatures during reciprocating sliding against carbon steel," *Wear*, vol. 330–331, pp. 209–222, May 2015, doi: 10.1016/J.WEAR.2015.01.026.

[74] P. V. Moghaddam, B. Prakash, E. Vuorinen, M. Fallqvist, J. M. Andersson, and J. Hardell, "High temperature tribology of TiAlN PVD coating sliding against 316L stainless steel and carbide-free bainitic steel," *Tribol. Int.*, vol. 159, no. September 2020, p. 106847, 2021, doi: 10.1016/j.triboint.2020.106847.

[75] J. M. Torralba, "(HIGH TEMPERATURE MATERIALS CHEMISTRY)," 2016. doi: 10.1134/S023501061901016X.

[76] W. Zhang, P. K. Liaw, and Y. Zhang, "A novel low-activation VCrFeTaxWx (x = 0.1, 0.2, 0.3, 0.4, and 1) high-entropy alloys with excellent heat-softening resistance," *Entropy*,

vol. 20, no. 12, 2018, doi: 10.3390/e20120951.

[77] J. K. Hong, I. S. Kim, C. Y. Park, and E. S. Kim, "Microstructural effects on the fretting wear of Inconel 690 steam generator tube," *Wear*, vol. 259, no. 1–6, pp. 349–355, Jul. 2005, doi: 10.1016/J.WEAR.2004.12.007.

[78] J. Li, Y. Lu, H. Zhang, and L. Xin, "Effect of grain size and hardness on fretting wear behavior of Inconel 600 alloys," *Tribol. Int.*, vol. 81, pp. 215–222, Jan. 2015, doi: 10.1016/J.TRIBOINT.2014.08.005.

[79] L. Xin, B. B. Yang, Z. H. Wang, J. Li, Y. H. Lu, and T. Shoji, "Microstructural evolution of subsurface on Inconel 690TT alloy subjected to fretting wear at elevated temperature," *Mater. Des.*, vol. 104, pp. 152–161, Aug. 2016, doi: 10.1016/J.MATDES.2016.05.030.

[80] X. Zhang, J. Liu, Z. Cai, J. Peng, M. Zhu, and P. Ren, "Experimental Study of the Fretting Wear Behavior of Incoloy 800 Alloy at High Temperature," *Tribol. Trans.*, vol. 60, no. 6, pp. 1110–1119, Nov. 2017, doi: 10.1080/10402004.2016.1261421.

[81] A. Günen, "Properties and High Temperature Dry Sliding Wear Behavior of Boronized Inconel 718," *Metall. Mater. Trans. A Phys. Metall. Mater. Sci.*, vol. 51, no. 2, pp. 927–939, 2020, doi: 10.1007/s11661-019-05577-3.

[82] T. Kurzynowski, I. Smolina, K. Kobiela, B. Kuźnicka, and E. Chlebus, "Wear and corrosion behaviour of Inconel 718 laser surface alloyed with rhenium," *Mater. Des.*, vol. 132, pp. 349–359, Oct. 2017, doi: 10.1016/J.MATDES.2017.07.024.

[83] Z. Xu *et al.*, "Tribological behaviors and microstructure evolution of Inconel 718 superalloy at mid-high temperature," *J. Mater. Res. Technol.*, vol. 14, pp. 2174–2184, 2021, doi: 10.1016/j.jmrt.2021.07.102.

[84] A. Shokrani, V. Dhokia, S. T. Newman, and R. Imani-Asrai, "An Initial Study of the Effect of Using Liquid Nitrogen Coolant on the Surface Roughness of Inconel 718 Nickel-Based Alloy in CNC Milling," *Procedia CIRP*, vol. 3, no. 1, pp. 121–125, Jan. 2012, doi: 10.1016/J.PROCIR.2012.07.022.

[85] J. Wanwan, Z. Chaoqun, J. Shuoya, T. Yingtao, W. Daniel, and L. Wen, "Wire Arc Additive Manufacturing of Stainless Steels: A Review," *Appl. Sci.*, vol. 10, p. 1563, 2020.

[86] J. Hardell and B. Prakash, "High-temperature friction and wear behaviour of different tool steels during sliding against Al–Si-coated high-strength steel," *Tribol. Int.*, vol. 41, no. 7, pp. 663–671, Jul. 2008, doi: 10.1016/J.TRIBOINT.2007.07.013.

[87] P. J. Blau, "Running-in: Art or engineering?," *J. Mater. Eng.*, vol. 13, pp. 47–53, Mar. 1991, doi: 10.1007/BF02834123.

[88] M. Calmunger, G. Chai, R. Eriksson, S. Johansson, and J. J. Moverare, "Characterization of Austenitic Stainless Steels Deformed at Elevated Temperature," *Metall. Mater. Trans. A Phys. Metall. Mater. Sci.*, vol. 48, no. 10, pp. 4525–4538, 2017, doi: 10.1007/s11661-017-4212-9.

[89] J. T. Burwell, "Survey of possible wear mechanisms," *Wear*, vol. 1, no. 2, pp. 119–141, Oct. 1957, doi: 10.1016/0043-1648(57)90005-4.

[90] S. Lu, Q. M. Hu, B. Johansson, and L. Vitos, "Stacking fault energies of Mn, Co and Nb alloyed austenitic stainless steels," *Acta Mater.*, vol. 59, no. 14, pp. 5728–5734, Aug. 2011, doi: 10.1016/J.ACTAMAT.2011.05.049.

[91] D. McIntyre, J. E. Greene, G. Håkansson, J.-E. Sundgren, and W.-D. Münz, "Oxidation of metastable single-phase polycrystalline Ti0.5Al0.5N films: Kinetics and mechanisms," *J. Appl. Phys.*, vol. 67, no. 3, pp. 1542–1553, Feb. 1990, doi: 10.1063/1.345664.

[92] C. Samuel. S, M. Arivarasu, and T. R. Prabhu, "High temperature dry sliding wear behaviour of laser powder bed fused Inconel 718," *Addit. Manuf.*, vol. 34, p. 101279, Aug. 2020, doi: 10.1016/J.ADDMA.2020.101279.

[93] Y. Lin *et al.*, "Effect of titanium addition on structure, corrosion resistance and mechanical properties of aluminum coatings on NdFeB by ion-beam-assisted magnetron sputtering," *Vacuum*, vol. 181, no. August, p. 109642, 2020, doi: 10.1016/j.vacuum.2020.109642.

[94] B. Syed *et al.*, "Morphology and microstructure evolution of Ti-50 at.% Al cathodes during cathodic arc deposition of Ti-Al-N coatings," *J. Appl. Phys.*, vol. 121, no. 24, 2017, doi: 10.1063/1.4990425.

[95] S. Koseki, K. Inoue, and H. Usuki, "Damage of physical vapor deposition coatings of cutting tools during alloy 718 turning," *Precis. Eng.*, vol. 44, pp. 41–54, Apr. 2016, doi: 10.1016/J.PRECISIONENG.2015.09.012.

[96] A. A. Vereschaka, S. N. Grigoriev, N. N. Sitnikov, and A. D. Batako, "Delamination and longitudinal cracking in multi-layered composite nano-structured coatings and their influence on cutting tool life," *Wear*, vol. 390–391, pp. 209–219, Nov. 2017, doi: 10.1016/J.WEAR.2017.07.021.

[97] N. TaşaltIn, S. Öztürk, N. KIlInç, H. Yüzer, and Z. Z. Öztürk, "Simple fabrication of hexagonally well-ordered AAO template on silicon substrate in two dimensions," *Appl. Phys. A Mater. Sci. Process.*, vol. 95, no. 3, pp. 781–787, 2009, doi: 10.1007/s00339-009-5071-z.

[98] S. Das and B. P. Swain, "Investigation of Titanium Aluminium Nitride (TiAlN): A Review," in *Advances in Electronics, Communication and Computing*, Singapore: Springer, 2018, pp. 147–158. doi: 10.1007/978-981-10-4765-7_16.

[99] C. Rynio, H. Hattendorf, J. Klöwer, and G. Eggeler, "The evolution of tribolayers during high temperature sliding wear," *Wear*, vol. 315, no. 1–2, pp. 1–10, Jul. 2014, doi: 10.1016/J.WEAR.2014.03.007.

[100] M. Moreno *et al.*, "Adhesive wear of TiAlN coatings during low speed turning of stainless steel 316L," *Wear*, vol. 524–525, p. 204838, Jul. 2023, doi: 10.1016/J.WEAR.2023.204838.

[101] K. H. Chuang and K. S. Hwang, "Free machining PIM 316L stainless steels," *Powder Metall.*, vol. 53, no. 1, pp. 57–61, 2010, doi: 10.1179/003258909X12502679013611.

[102] S. PalDey and S. C. Deevi, "Single layer and multilayer wear resistant coatings of (Ti,Al)N: a review," *Mater. Sci. Eng. A*, vol. 342, no. 1–2, pp. 58–79, Feb. 2003, doi:

10.1016/S0921-5093(02)00259-9.

[103] A. Joshi and H. S. Hu, "Oxidation behavior of titanium-aluminium nitrides," *Surf. Coatings Technol.*, vol. 76–77, no. PART 2, pp. 499–507, Dec. 1995, doi: 10.1016/0257-8972(95)02566-9.

[104] K. Bobzin, "High-performance coatings for cutting tools," *CIRP J. Manuf. Sci. Technol.*, vol. 18, pp. 1–9, Aug. 2017, doi: 10.1016/J.CIRPJ.2016.11.004.

Appendix A: Repeatability for Inconel 718 and $Ti_{60}Al_{40}N$

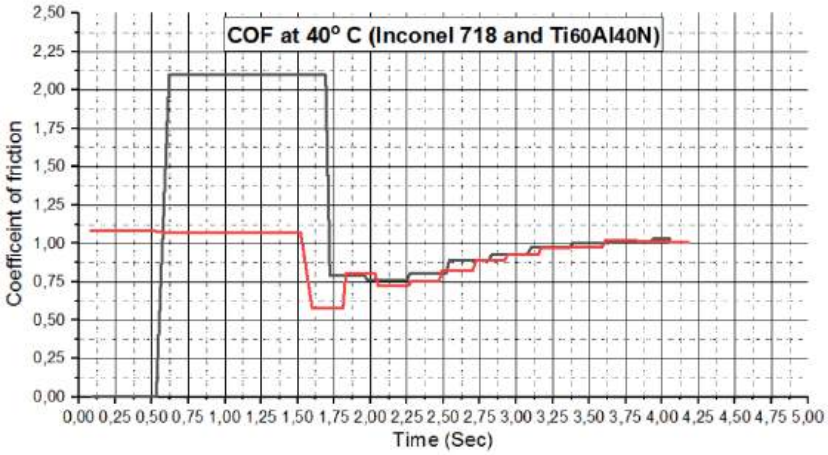

Figure 45: COF repeatability test for Inconel 718 and $Ti_{60}Al_{40}N$ at 40°C

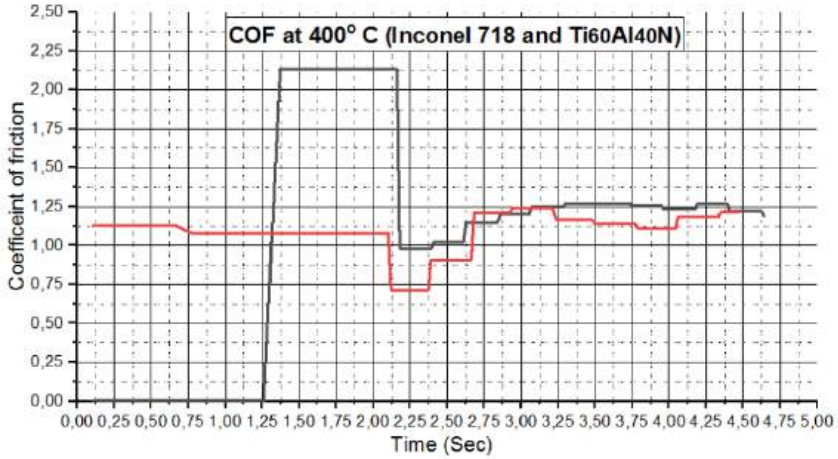

Figure 46: COF repeatability test for Inconel 718 and $Ti_{60}Al_{40}N$ at 400°C

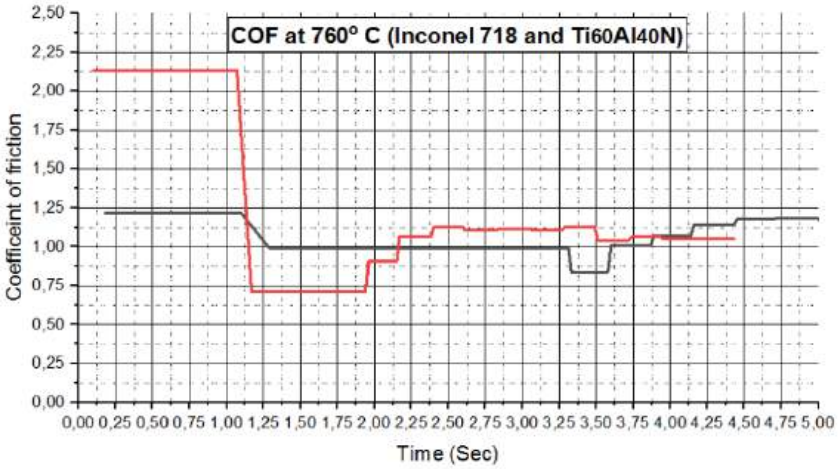

Figure 47: COF repeatability test for Inconel 718 and $Ti_{60}AL_{40}N$ at 760° C

Appendix B: Repeatability for SS 316L and $Ti_{60}Al_{40}N$

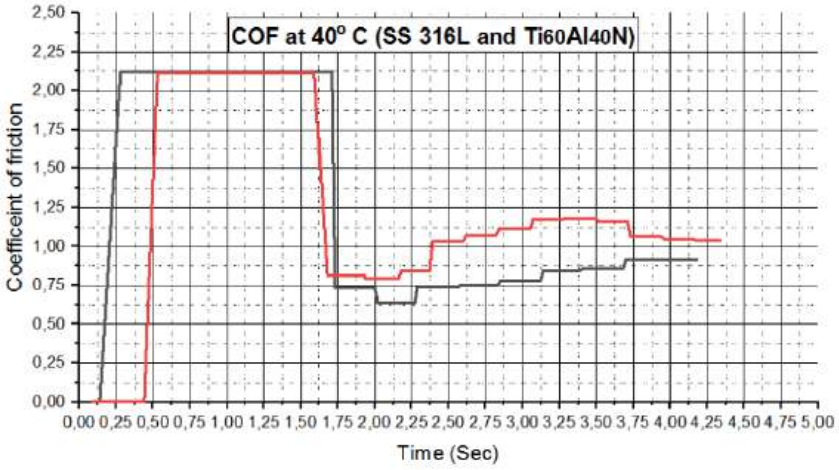

Figure 48: COF repeatability test for SS 316L and $Ti_{60}Al_{40}N$ at 40° C

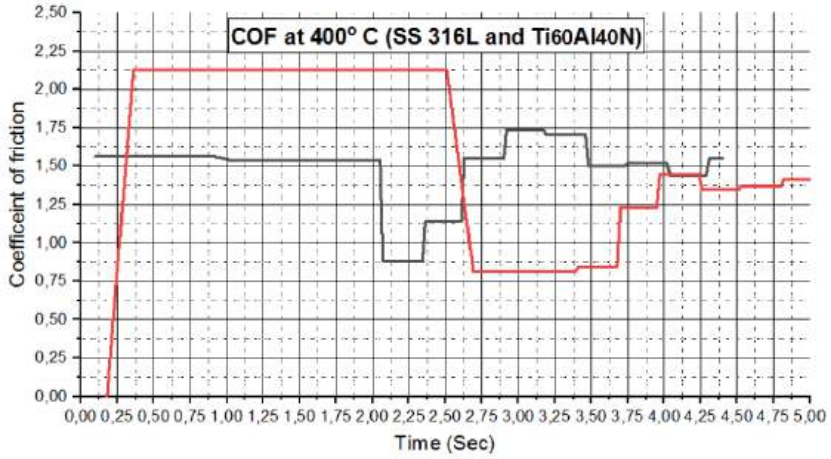

Figure 49: COF repeatability test for SS 316L and $Ti_{60}Al_{40}N$ at 400° C

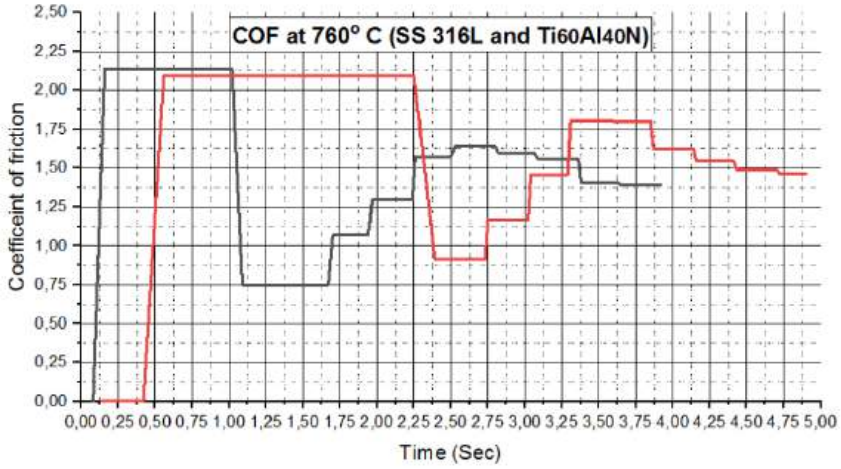

Figure 50: COF repeatability test for SS 316L and $Ti_{60}Al_{40}N$ at 760° C

Appendix C: Repeatability for Inconel 718 and $Ti_{40}Al_{60}N$

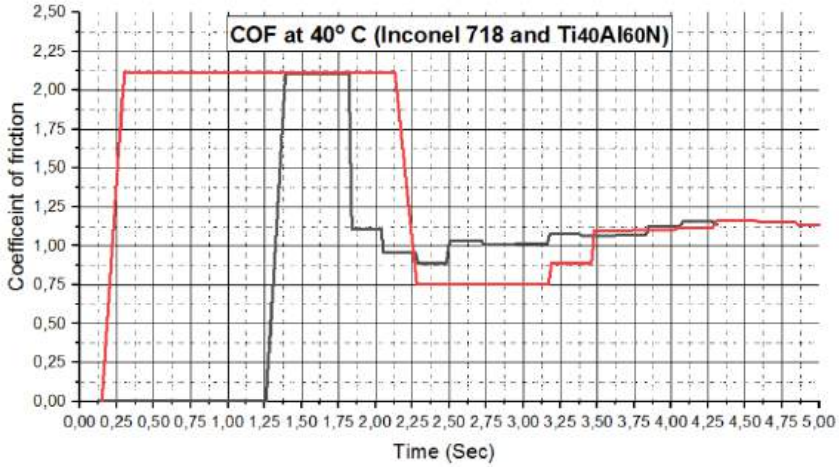

Figure 51: COF repeatability test for Inconel 718 and $Ti_{40}Al_{60}N$ at 40° C

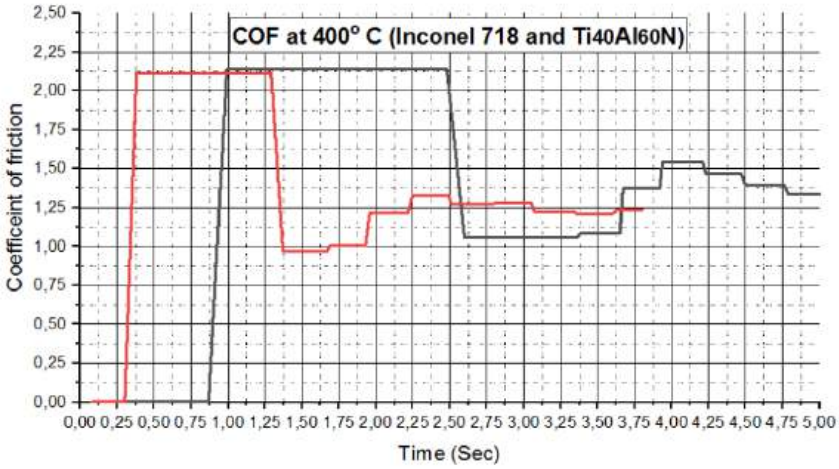

Figure 52: COF repeatability test for Inconel 718 and $Ti_{40}Al_{60}N$ at 400° C

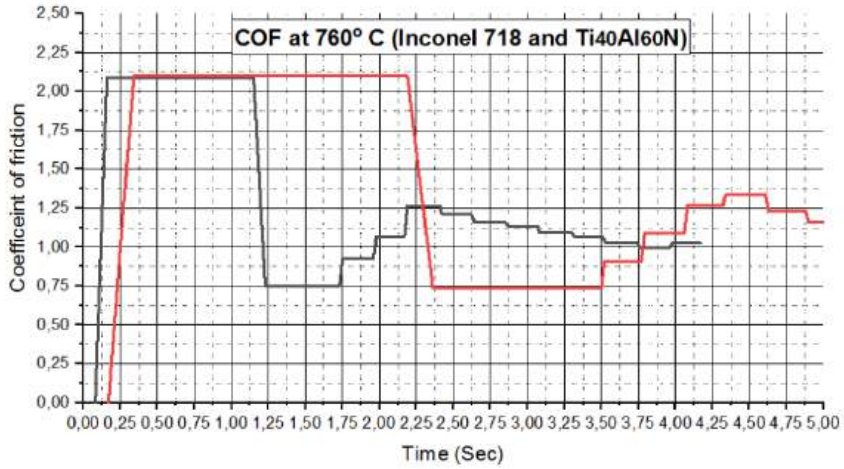

Figure 53: COF repeatability test for Inconel 718 and $Ti_{40}Al_{60}N$ at 760° C

Appendix D: Repeatability for SS 316L and $Ti_{40}Al_{60}N$

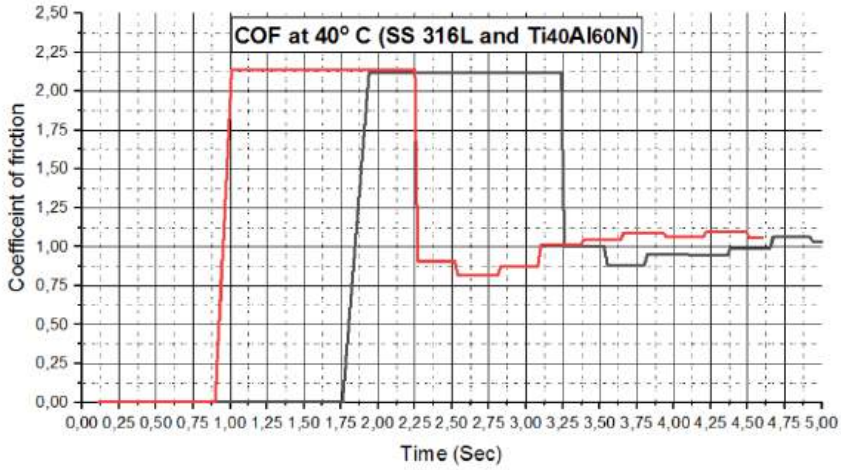

Figure 54: COF repeatability test for SS 316L and $Ti_{40}Al_{60}N$ at 40° C

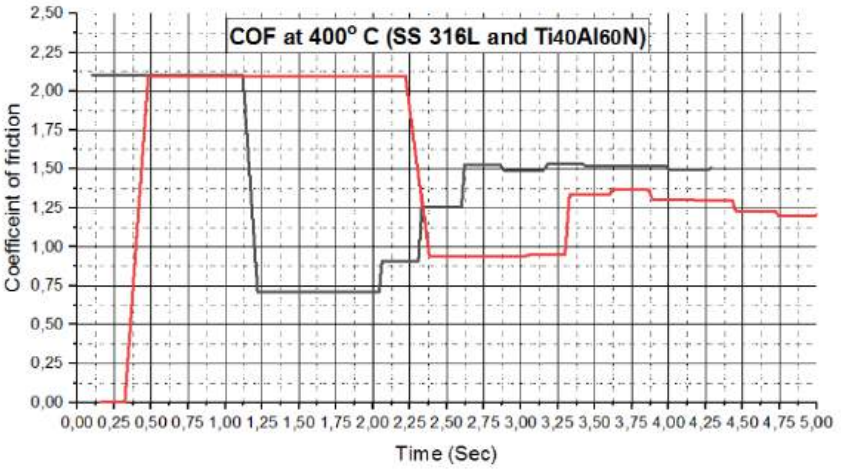

Figure 55: COF repeatability test for SS 316L and $Ti_{40}Al_{60}N$ at 400° C

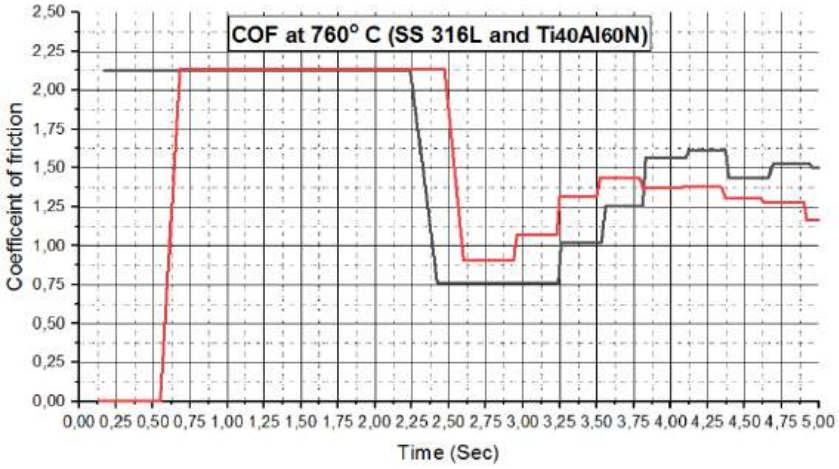

Figure 56: COF repeatability test for SS 316L and $Ti_{40}Al_{60}N$ at 760° C

Mr

ORIGINALITY REPORT

16%	12%	10%	3%
SIMILARITY INDEX	INTERNET SOURCES	PUBLICATIONS	STUDENT PAPERS

PRIMARY SOURCES

1	www.essays.se Internet Source	3%
2	Pouria Valizadeh Moghaddam, Braham Prakash, Esa Vuorinen, Mikael Fallqvist, Jon M. Andersson, Jens Hardell. "High temperature tribology of TiAlN PVD coating sliding against 316L stainless steel and carbide-free bainitic steel", Tribology International, 2021 Publication	1%
3	ltu.diva-portal.org Internet Source	1%
4	Encyclopedia of Tribology, 2013. Publication	1%
5	dspace.dtu.ac.in:8080 Internet Source	1%
6	www.dspace.dtu.ac.in:8080 Internet Source	<1%
7	www.coursehero.com Internet Source	<1%
8	de.overleaf.com Internet Source	<1%
9	C. Courbon, M. Fallqvist, J. Hardell, R. M Saoubi, B. Prakash. "Adhesion tendency of PVD TiAlN coatings at elevated temperatures during reciprocating sliding against carbon steel", Wear, 2015 Publication	<1%

10	dergipark.ulakbim.gov.tr Internet Source	<1 %
11	macsphere.mcmaster.ca Internet Source	<1 %
12	www.mdpi.com Internet Source	<1 %
13	libweb.kpfu.ru Internet Source	<1 %
14	www.researchgate.net Internet Source	<1 %
15	Zhibiao Xu, Zhengyu Huang, Jun Zhang, Xing Xu, Peng Li, Fenghua Su, Minhao Zhu. "Tribological behaviors and microstructure evolution of Inconel 718 superalloy at mid-high temperature", Journal of Materials Research and Technology, 2021 Publication	<1 %
16	link.springer.com Internet Source	<1 %
17	kth.diva-portal.org Internet Source	<1 %
18	www.diva-portal.org Internet Source	<1 %
19	"Advances in Computational Methods in Manufacturing", Springer Science and Business Media LLC, 2019 Publication	<1 %
20	journal.hep.com.cn Internet Source	<1 %
21	Shuho Koseki, Kenichi Inoue, Katsuhiko Sekiya, Shigekazu Morito, Takuya Ohba, Hiroshi Usuki. "Wear mechanisms of PVD-	<1 %

	coated cutting tools during continuous turning of Ti-6Al-4V alloy", Precision Engineering, 2017 Publication	
22	Anirban Naskar, A.K. Chattopadhyay. "Investigation on flank wear mechanism of CVD and PVD hard coatings in high speed dry turning of low and high carbon steel", Wear, 2018 Publication	<1 %
23	www.science.gov Internet Source	<1 %
24	Ali Günen. "Properties and High Temperature Dry Sliding Wear Behavior of Boronized Inconel 718", Metallurgical and Materials Transactions A, 2019 Publication	<1 %
25	Chetan, S. Ghosh, P.V. Rao. "Performance evaluation of deep cryogenic processed carbide inserts during dry turning of Nimonic 90 aerospace grade alloy", Tribology International, 2017 Publication	<1 %
26	Submitted to Curtin University of Technology Student Paper	<1 %
27	Thakur, A., and S. Gangopadhyay. "State-of-the-art in surface integrity in machining of nickel-based super alloys", International Journal of Machine Tools and Manufacture, 2016. Publication	<1 %
28	purehost.bath.ac.uk Internet Source	<1 %

29	Amit Bansal, Apurbba Kumar Sharma, Shantanu Das, Pradeep Kumar. "On microstructure and strength properties of microwave welded Inconel 718/ stainless steel (SS-316L)", Proceedings of the Institution of Mechanical Engineers, Part L: Journal of Materials: Design and Applications, 2016 Publication	<1 %
30	open.library.ubc.ca Internet Source	<1 %
31	Abhishek Singh, S. Ghosh, S. Aravindan. "State of art for sustainable machining of nickel-based alloys using coated and uncoated tools and machining of high strength materials using surface modified cutting tools", Tribology International, 2022 Publication	<1 %
32	Murat Sarıkaya, Munish Kumar Gupta, Italo Tomaz, Danil Yu Pimenov et al. "A state-of-the-art review on tool wear and surface integrity characteristics in machining of superalloys", CIRP Journal of Manufacturing Science and Technology, 2021 Publication	<1 %
33	Dahu Zhu, Xiaoming Zhang, Han Ding. "Tool wear characteristics in machining of nickel-based superalloys", International Journal of Machine Tools and Manufacture, 2013 Publication	<1 %
34	uu.diva-portal.org Internet Source	<1 %
35	Anselmo Eduardo Diniz, Álisson Rocha Machado, Janaina Geilser Corrêa. "Tool wear mechanisms in the machining of steels and	<1 %

	stainless steels", The International Journal of Advanced Manufacturing Technology, 2016 Publication	
36	e-space.mmu.ac.uk Internet Source	<1 %
37	bura.brunel.ac.uk Internet Source	<1 %
38	Submitted to atharvacoe Student Paper	<1 %
39	eprints.nottingham.ac.uk Internet Source	<1 %
40	vital.seals.ac.za:8080 Internet Source	<1 %
41	Submitted to Indian Institute of Technology, Bombay Student Paper	<1 %
42	Laizhu Jiang, Hannu HÄnninen, Jukka Paro, Veijo Kauppinen. "Active wear and failure mechanisms of TiN-Coated high speed steel and tin-coated cemented carbide tools when machining powder metallurgically made stainless steels", Metallurgical and Materials Transactions A, 1996 Publication	<1 %
43	dl-asminternational-org_proxy.dotlib.com.br Internet Source	<1 %
44	Mi, X., Z.B. Cai, X.M. Xiong, H. Qian, L.C. Tang, Y.C. Xie, J.F. Peng, and Min-hao Zhu. "Investigation on fretting wear behavior of 690 alloy in water under various temperatures", Tribology International, 2016. Publication	<1 %
45	dspace.upt.ro Internet Source	<1 %

46	hal.science Internet Source	<1 %
47	journals.pan.pl Internet Source	<1 %
48	www.hindawi.com Internet Source	<1 %
49	Jinxing Kong, Zhihui Xia, Dongming Xu, Ning He. "Investigation on notch wear mechanism in finish turning pure iron material with uncoated carbide tools under different cooling/lubrication conditions", The International Journal of Advanced Manufacturing Technology, 2015 Publication	<1 %
50	Submitted to Tennessee Technological University Student Paper	<1 %
51	ir.knust.edu.gh Internet Source	<1 %
52	www.researchsquare.com Internet Source	<1 %
53	Kuniaki Dohda, Christine Boher, Farhad Rezai-Aria, Numpon Mahayotsanun. "Tribology in metal forming at elevated temperatures", Friction, 2015 Publication	<1 %
54	Rui Wang, Dayong Yang, Wei Wang, Furui Wei, Yuwei Lu, Yuqi Li. "Tool Wear in Nickel-Based Superalloy Machining: An Overview", Processes, 2022 Publication	<1 %
55	Sebbe, Naiara Poli Veneziani. "Estudo Experimental da Influência do Comprimento	<1 %

de Corte no Comportamento de Desgaste de Ferramentas com Revestimento de TiN/TiALN Durante Fresagem de Inconel 718", Instituto Politecnico do Porto (Portugal), 2024
Publication

56	www.ncbi.nlm.nih.gov Internet Source	<1 %
57	Submitted to Cranfield University Student Paper	<1 %
58	Submitted to Ohio University Student Paper	<1 %
59	Submitted to University of Sheffield Student Paper	<1 %
60	"Research Needs in Mechanical Systems—Report of the Select Panel on Research Goals and Priorities in Mechanical Systems", Journal of Tribology, 1984 Publication	<1 %
61	Lihua Yu, Jian Chen, Hongbo Ju, Hongzhi Dong, Hongjian Zhao. "Influence of Al content on microstructure, mechanical and tribological properties of Ti-W-Al-N composite films", Vacuum, 2017 Publication	<1 %
62	Tian, X., J. Zhao, Y. Dong, N. Zhu, J. Zhao, and A. Li. "A comparison between whisker-reinforced alumina and SiAlON ceramic tools in high-speed face milling of Inconel 718", Proceedings of the Institution of Mechanical Engineers Part B Journal of Engineering Manufacture, 2014. Publication	<1 %
63	d21zja6o12zyp0.cloudfront.net Internet Source	<1 %

64	dspace.gazi.edu.tr Internet Source	<1 %
65	forgottenbooks.com Internet Source	<1 %
66	Submitted to iGroup Student Paper	<1 %
67	mdpi-res.com Internet Source	<1 %
68	scholar.sun.ac.za Internet Source	<1 %
69	Anderson Clayton Alves de Melo. "Influence of cutting tool geometry, feed rate and cutting fluid on the machinability of Inconel 751", International Journal of Machining and Machinability of Materials, 2011 Publication	<1 %
70	Hayama, Hiroki, Hiroki Kiyota, Fumihiro Itoigawa, and Takashi Nakamura. "Size Effect in Machining on Initial Tool Wear in Heat-Resistant Alloy Cutting", Key Engineering Materials, 2015. Publication	<1 %
71	Navneet Khanna, Prassan Shah, Chetan. "Comparative analysis of dry, flood, MQL and cryogenic CO2 techniques during the machining of 15-5-PH SS alloy", Tribology International, 2020 Publication	<1 %
72	Ravindra Ishwar Badiger, S Narendranath, M S Srinath. "Microstructure and mechanical properties of Inconel-625 welded joint developed through microwave hybrid heating", Proceedings of the Institution of	<1 %

Mechanical Engineers, Part B: Journal of Engineering Manufacture, 2017
Publication

73	Tianxiang Wang, Xuming Zha, Fengbiao Chen, Jue Wang, Liangliang Lin, Hong Xie, Fengtian Lin, Feng Jiang. "Research on cutting performance of coated cutting tools by a new impact test method considering contact stress condition caused by segmented chips", Journal of Manufacturing Processes, 2021 Publication	<1 %
74	Yadav, Rajiv Kumar, Kumar Abhishek, and Siba Sankar Mahapatra. "A simulation approach for estimating flank wear and material removal rate in turning of Inconel 718", Simulation Modelling Practice and Theory, 2015. Publication	<1 %
75	mit.imt.si Internet Source	<1 %
76	researcharchive.lincoln.ac.nz Internet Source	<1 %
77	www.degruyter.com Internet Source	<1 %
78	www.frontiersin.org Internet Source	<1 %
79	www2.mdpi.com Internet Source	<1 %
80	123dok.net Internet Source	<1 %
81	E.O. Ezugwu, Z.M. Wang, A.R. Machado. "The machinability of nickel-based alloys: a review", Journal of Materials Processing Technology, 1999	<1 %

Publication

82	Janaina Geisler Corrêa, Rolf Bertrand Schroeter, Álisson Rocha Machado. "Tool life and wear mechanism analysis of carbide tools used in the machining of martensitic and supermartensitic stainless steels", Tribology International, 2017 Publication	<1 %
83	Kose, E.. "The effects of the feed rate on the cutting tool stresses in machining of Inconel 718", Journal of Materials Processing Tech., 20080121 Publication	<1 %
84	Pusavec, Franci, Ashish Deshpande, Shu Yang, Rachid M'Saoubi, Janez Kopac, Oscar W. Dillon, and Ibrahim S. Jawahir. "Sustainable Machining of High Temperature Nickel Alloy – Inconel 718: Part 1 – Predictive Performance Models", Journal of Cleaner Production, 2014. Publication	<1 %
85	T. S. Srivatsan, T. S. Sudarshan, K. Manigandan. "Manufacturing Techniques for Materials - Engineering and Engineered", CRC Press, 2018 Publication	<1 %
86	Uttkarsh S. Patel, Sushant K. Rawal, A.F.M. Arif, Stephen C. Veldhuis. "Influence of secondary carbides on microstructure, wear mechanism, and tool performance for different cermet grades during high-speed dry finish turning of AISI 304 stainless steel", Wear, 2020 Publication	<1 %
87	core.ac.uk Internet Source	<1 %

88	downloads.hindawi.com Internet Source	<1 %
89	ebiltegia.mondragon.edu Internet Source	<1 %
90	hv.diva-portal.org Internet Source	<1 %
91	m.hisupplier.com Internet Source	<1 %
92	portal.research.lu.se Internet Source	<1 %
93	publikationen.bibliothek.kit.edu Internet Source	<1 %
94	pure.mpg.de Internet Source	<1 %
95	riunet.upv.es Internet Source	<1 %
96	shura.shu.ac.uk Internet Source	<1 %
97	webthesis.biblio.polito.it Internet Source	<1 %
98	www.archivesmse.org Internet Source	<1 %
99	www.mechanics-industry.org Internet Source	<1 %
100	www.scribd.com Internet Source	<1 %
101	www.tandfonline.com Internet Source	<1 %
102	www.vtt.fi Internet Source	<1 %

Exclude quotes	On	Exclude matches	< 9 words
Exclude bibliography	On		